TECHNISCHE
UNIVERSITÄT
WIEN
Vienna University of Technology

AUTOMATION & CONTROL INSTITUTE
INSTITUT FÜR AUTOMATISIERUNGS-
& REGELUNGSTECHNIK

High-frequency PWM amplifier for high precision motion

DIPLOMARBEIT

Ausgeführt zum Zwecke der Erlangung des akademischen Grades eines
Diplom-Ingenieurs (Dipl.-Ing.)

unter der Leitung von

Univ.-Prof. Dr.sc.techn. Georg Schitter
Ito Shingo, Projektass. Dr.techn. MSc
Riel Thomas, Univ.Ass. Dipl.-Ing. BSc

eingereicht an der
Technischen Universität Wien
Fakultät für Elektrotechnik und Informationstechnik
Institut für Automatisierungs- und Regelungstechnik

von

Dijana Šibenik, BSc
Matrikelnummer: 01529592
Wien, Österreich

Wien, im Januar 2020

Advanced Mechatronic Systems Group
Gußhausstraße 27-29, A-1040 Wien, Internet: http://www.acin.tuwien.ac.at

Acknowledgment

Writing thesis was the most demanding task I had during my studies and it would not be possible to realize it without support of many people. First I would like to thank my project advisors Shingo Ito and Thomas Riel for the technical support and knowledge they shared with me. Also I would like to thank Professor Schitter who is responsible for this thesis and made it possible in the first place. Many thanks to all of my friends and colleagues for their support, suggestions and discussions during this time. Finally, I can not express how much I am grateful to my family: my father Mirko, mother Edina and brother Goran. It is for their support and sacrifice that I was able to do my studies in Austria. They were always there for me, day or night. Thank you!

Abstract

High quality motion with nanometer resolution is indispensable in many systems such as atomic force microscopes and high-precision 3D- printers. In these systems, Lorentz actuators or piezoelectric actuators are typically utilized to satisfy the requirements on the positioning resolution and bandwidth, and they are usually driven by linear power amplifiers. They have low noise for high-precision motion; however, their energy efficiency is low, resulting in energy dissipation and a cooling system requirement. Although the energy efficiency can be improved by using switching power amplifiers, they generate current ripples that impair motion precision.

To drive high-precision actuators in an energy efficient way without degrading the motion resolution, this thesis investigates the feasibility to utilize switching power amplifiers based on Gallium Nitride (GaN) transistors, which enable a higher switching frequency in comparison with conventional silicon-based transistors. For the experimental investigation, a switching power amplifier is developed, consisting of a PWM generator, logic and dead-time adjustment circuit, an output stage and an LC-filter. Evaluation of the developed amplifier is conducted with inductive load and piezoelectric actuator.

Experimental results with the inductive load show that the increase of the switching frequency from 20 kHz to 1 MHz decreases the current ripple of the coil current by a factor of 13 while power dissipation is constantly low. However, the energy dissipation analysis reveals high energy losses when the developed power amplifier is used for driving the piezoelectric actuator. Analysis shows that cause for these losses is the hard switching effect occurring when amplifier is used for driving a capacitive load. Experimental results also show that the high-frequency switching is beneficial for a high positioning bandwidth and reduction of a standard deviation of voltage on the piezoelectric actuator up to switching frequency of 450 kHz.

Zusammenfassung

Hochwertige Bewegungen mit Nanometerauflösung sind in vielen Systemen wie Rasterkraftmikroskopen und Hochpräzisions 3D-Druckern unersetzlich. In diesen Systemen werden üblicherweise Lorentz-Aktuatoren oder Piezoaktoren verwendet, sodass die Anforderungen auf Auflösung und Bandbreite erfüllt sind. Sie werden normalerweise durch lineare Leistungsverstärker angetrieben. Diese sind rauscharm für hochpräzise Bewegungen. Ihre Energieeffizienz ist jedoch gering und die Energieverluste sind hoch, weshalb sie Kühlsysteme erfordern. Die Energieeffizienz kann durch die Verwendung von Schaltleistungsverstärkern verbessert werden, welche jedoch Stromrippel erzeugen, die die Bewegungspräzision beeinträchtigen.

Um hochpräzise Aktuatoren energieeffizient anzusteuern, ohne die Bewegungsauflösung zu beeinträchtigen, wird in dieser Arbeit die Möglichkeit untersucht, Schaltleistungsverstärker auf Basis von Galliumnitrid-Transistoren (GaN-Transistoren) einzusetzen, die im Vergleich zu herkömmlichen Transistoren auf Siliziumbasis eine höhere Schaltfrequenz ermöglichen. Für die experimentelle Untersuchung wird ein Schaltleistungsverstärker bestehend aus einem PWM-Generator, einer Logik- und einer Totzeit-Einstellschaltung, Endstufe und einem LC-Filter entwickelt. Die Auswertung des entwickelten Verstärkers erfolgt mit induktiver Last und einem Piezoaktor.

Experimentelle Ergebnisse mit der induktiven Last zeigen, dass sich bei der Erhöhung der Schaltfrequenz von 20 kHz bis 1 MHz, der Stromrippel des Spulenstroms 13 mal verringert, während Energieverluste konstant niedrig bleiben. Die Analyse zeigt jedoch hohe Energieverluste, wenn der entwickelte Leistungsverstärker zur Ansteuerung des Piezoaktors eingesetzt ist. Aus den Ergebnissen der Analyse wurde festgestellt, dass die Ursache für diese Verluste der Hart-Schalt-Effekt ist, der auftritt, wenn der Verstärker zur Ansteuerung einer kapazitiven Last verwendet wird. Experimentelle Ergebnisse zeigen auch, dass das Hochfrequenzschalten für eine hohe Positionierbandbreite und eine Reduzierung der Standardabweichung der Spannung am Piezoaktor bis zur Schaltfrequenz von 450 kHz günstig ist.

Contents

List of Figures

List of Tables

Acronyms

AFM	Atomic Force Microscopy
BGA	Ball Grid Array
EMI	Electromagnetic Interference
FET	Field Effect Transistor
FoM	Figure of Merit
GaN	Gallium Nitride
IC	Integrated Circuit
IDS	Industrial Displacement Sensor
IGBT	Insulated-gate bipolar transistor
LVTTL	Low-Voltage Transistor-Transistor-Logic
PCB	Printed Circuit Board
PWM	Puls Width Modulation
RMS	Root-Mean Square
SiC	Silicon Carbide
SMA	SubMiniature version A
SMD	Surface Mount Device
THD	Total Harmonic Distortion

CHAPTER 1

Introduction

1.1 Background

Many systems require highly precise motion for industrial application and scientific instrumentation. Some of the examples include Atomic Force Microscopy (AFM) [2], lithographic equipment [3] and additive manufacturing [4]. These systems typically use Lorentz actuators or piezoelectric actuators. They are driven by appropriate amplifiers, which influence the achievable motion precision and energy efficiency of the resulting systems.

AFM is used for imaging and manipulating on small-scale level with high resolution [5]. For highest achievable performance piezoelectric actuators are commonly used in AFMs to scan the sample [2]. Although piezoelectric actuators achieve high bandwidth and subnanometer resolution [6] to achieve high bandwidth of the system, other devices used in the system also need to meet the requirements. One of challenges in AFM systems is the power amplifier that drives the piezoelectric actuator, which is a capacitive load [7]. All amplifiers have limited bandwidth and their bandwidth often depends on the output impedance and changes with different load impedance. To achieve high scanning speed without sacrificing the positioning resolution, it is desirable to develop custom-made power amplifier [8]. Positioning resolution is affected by noise floor of the power amplifiers [8]. Therefore for the highest system performance of the AFM, the amplifier bandwidth needs to be larger than 10 kHz and noise lower than $10\,mV_{pp}$ [2].

In case of laser scanning systems, such as fast steering mirrors [9] or galvanometer scanners [10], electromagnetic actuators such as voice coil actuators are utilized for example for imaging and additive manufacturing. Such electromagnetic actuators are regarded as an inductive load and driven by a power amplifier, which needs to achieve a sufficiently high bandwidth and sufficiently low noise for required high-speed motion with high resolution.

As discussed above, power amplifiers in high precision motion systems need to

achieve high bandwidth and low noise for the high performance. They also need to have high energy efficiency, such that the power consumption and the heating of components in the power amplifier is reduced. In order to satisfy these different requirements, there are different types of amplifiers as discussed in Secton 1.2.

1.2 State of the Art

1.2.1 Linear Power Amplifiers

Most commonly used amplifiers in high precision systems are linear power amplifiers. Power amplifiers are designed to deliver high output voltage and high output current to the load. Figure 1.1 shows one type of linear power amplifier. This amplifier consists of two transistors, which are used to amplify input signal V_{in}. Linear power amplifiers are designed in a way that transistors operate in linear region of their voltage-current characteristics. Transistors are connected in series between input and output [11], and an output signal is proportional to an input signal. In ON state there is a certain voltage drop between transistor Drain and Source V_{DS}. Since the transistor is conducting current I_D, it is dissipating power $P = V_{DS}I_D$.

Linear power amplifiers have high accuracy, since they generate smooth output voltage signal which is proportional to input voltage signal. Ideally, they do not have any nonlinearities caused by internal properties, such as dynamic, offset, power supply limitations and deviations [3]. In reality this in not the case, but in many applications they can be considered as ideal [3]. All nonlinearities which are reproducible and deterministic, can be compensated [3].

Although accuracy of linear power amplifiers is high, their power efficiency is low. Different types of linear power amplifiers have different current conducting intervals, during which they dissipate power $P = V_{DS}I_D$. For linear power amplifier with transistors contantly in ON state conducting current, maximum energy efficiency of a power amplifier is 40% [12]. For other linear power amplifiers using transistors which are only periodically conducting current, increase in energy efficiency has as a consequence increase in the output signal nonlinearity [13]. Because of a low power efficiency transistors are heating, and these amplifiers need cooling systems. For purely reactive, inductive or capacitive load, the power dissipation in a linear power amplifiers increases, because the load current is out of phase with the voltage [3]. Their low energy efficiency makes them unsuitable for driving high voltage and current actuators, such as piezoelectric and Lorentz actuator. Power amplifier size is related to power efficiency, because large heat dissipation needs to be reduced by large cooling systems. Low power efficiency increases the size of the power amplifier and the system.

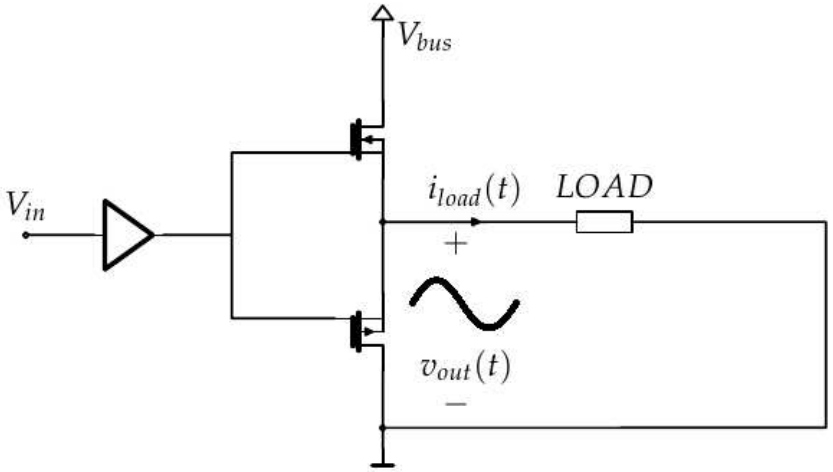

Figure 1.1: Linear power amplifier

1.2.2 Switching Power Amplifiers

Switching power amplifiers main characteristics is that conducting interval is much shorter than the time period of the input signal. The most simple example of a switching power amplifier is a class-D amplifier, as shown in Figure 1.2. It consists of two transistors, in the same manner as linear power amplifier, but the working principle of the switching amplifier is different. A major difference can be seen in the form of the output voltage signal v_{out}. A class-D amplifier is a half-bridge, and it operates according to Puls Width Modulation (PWM) principle [3]. This means that transistors operate in cutoff or saturation region of the transistors voltage-current characteristic. When a transistor is in ON state, it operates in saturation region, and it can be considered that voltage $V_{DS} = 0\,\text{V}$. In the transistor OFF state, current through transistor is $I_D = 0\,\text{A}$. To restore the input signal wave shape switching amplifiers need filters. These filters damp the high frequency harmonics from the output signal v_{out}, such that they can be neglected in comparison to ground frequency signal.

The power dissipation of transistors in switching power amplifiers, calculated as $P = V_{DS}I_D$, can be in both ON and OFF state considered zero, thus switching power amplifiers have high energy efficiency. This means that switching power amplifiers can deliver high current and voltage with reduced energy losses. Nanopositioning systems could benefit from switching power amplifiers since they employ high voltage and current actuators. Switching power amplifiers are desirable when driving piezoelectric load, since piezoelectric actuators require a high voltage of more than tens of Volts and switching amplifiers have a possibility to recover energy in case of field reduction [14].

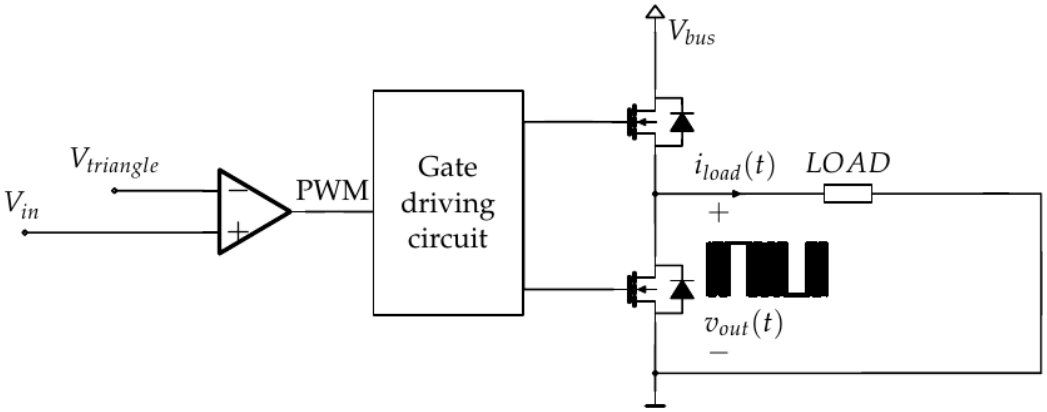

Figure 1.2: Class-D switching power amplifier

Main disadvantages of using switching amplifiers in nanopositioning systems are high current ripple and output signal distortion caused by high frequency harmonics. Although damped by the filter, these high frequency harmonics represent disturbance, which is large enough to corrupt the output signal accuracy. Current ripple is a consequence of PWM principle and an output signal distortion is mainly caused by a dead-time T_d. The dead-time needs to be introduced, to protect the transistors and the power supply of shoot-through currents. Parasitic capacitance is inherent property of every transistor and it is shown in Figure 1.3. It limits the slew rate of the output signal, so without dead-time (T_d) between driving signals V_{GS} of the high and low side transistor $G1$ and $G2$ respectively, as shown in Figure 1.4, it would come to shoot-through currents which could short-circuit the power supply. The gate driving signals have to be non-overlapping.

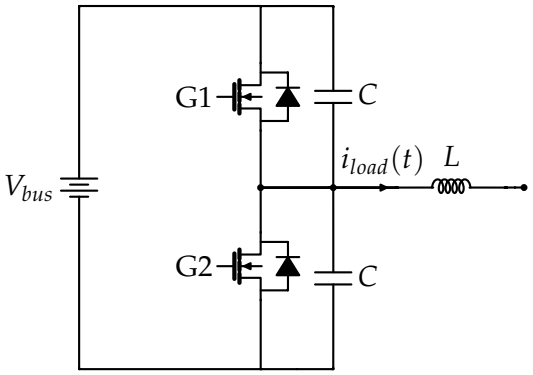

Figure 1.3: Parasitic capacitance, drawn based on [15]

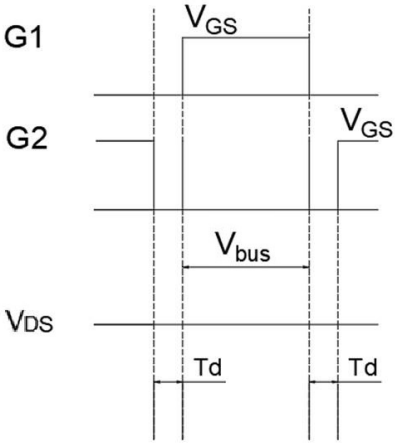

Figure 1.4: Dead time, drawn based on [16]

Although energy efficiency of class-D amplifiers is 100% ideally, in reality there are

certain energy losses caused due to output voltage rise and fall time and $R_{DS(ON)}$ resistance. During the rise and fall time there is a certain power dissipation because both current and voltage are different from zero, and during the transistor ON state there is a small voltage drop V_{DS} due to $R_{DS(ON)} \neq 0$. These losses cause heating of the transistors, which depend on transistor types as follows.

Silicon-Based Switching Power Amplifiers

Silicon-based switching power amplifiers are amplifiers with switches made of silicon semiconductor. MOSFETs are one of the most spread power switches. MOSFETs, where MOS stands for Metal Oxide Silicon, are named after silicon semiconductor from which they are made of.

Silicon is the widest spread semiconductor used in electronics and it is used to make different switching components, which are employed for different applications [17]. Applications which require very high output powers at low switching frequencies employ thyristors and Insulated-gate bipolar transistor (IGBT) [17]. To deliver high power, in applications such as pulsed power supplies, where switching frequencies need to be higher MOSFETs are used [17]. Switching frequencies of typical MOSFETs are higher than those of thyristors and the IGBTs and they are up to 100 kHz [17].

Although higher than those of thyristors and the IGBTs, switching frequencies of typical MOSFETs are still relatively low, because they are limited by the parasitic capacitance which introduces a finite output voltage change dV/dt. In this case, current ripple and influence of high frequency harmonics is high. Consequently, they are rarely selected for precision motion control applications, because they have high requirements on output distortion and noise [18].

GaN-Based Switching Power Amplifiers

Development of new technologies has made switching power amplifiers more attractive for different high power and low noise applications. These new technologies allow high switching frequency, hence besides high efficiency these amplifiers can have low Total Harmonic Distortion (THD) [18]. Components used for developing these switching power amplifiers are smaller, and in applications where there is no need for cooling systems, these amplifiers are smaller and more compatible.

One of these newly developed technologies is a Gallium Nitride (GaN) Field Effect Transistor (FET) transistor. GaN FETs are processed using standard CMOS equipment, hence new technologies are not needed for their production. Figure of Merit (FoM) for the FET transistors is the product of $R_{DS(ON)}$ and gate charge: $R_{DS(ON)} \cdot Q_g$. GaN transistors have a very good performance because exceptionally high electron mobility and low temperature coefficient results in very low $R_{DS(ON)}$, exceptionally low gate charge (Q_g) and zero source-drain recovery charge (Q_{RR}). These improvements result in short ON-time and high power efficiency of transistors. [19]

Not only the GaN-based technologies have made higher switching frequencies possible. There are also Silicon Carbide (SiC) technologies, as well as new silicon MOSFETs. In [20] efficiency comparison of the three technologies has been done. It is shown that efficiency of GaN FET is higher than the efficiency of the SiC and conventional MOSFET, and it reaches more than 95% [20]. This makes the GaN FET a perfect candidate to consider for high energy efficiency application.

Due to relatively new technology, not all application fields have been yet investigated. A lot of research is carried out about dynamic *ON*-resistance [21], [22] and parasitic capacitance hysteresis [23], [24] of the GaN FET. By now, performance of newly developed transistors in power amplifiers with inductive and resistive load has been investigated, where the load current can be considered constant during one PWM cycle [18], [25]. However, GaN-based driver for high resolution positioning of capacitive loads is not well-investigated yet.

1.2.3 Research Objective

Although there are different types of power amplifiers, it is difficult to satisfy all the requirements simultaneously, as discussed above. Due to the smooth output voltage, a linear amplifier is ideal to drive a high-precision actuator. However, a linear amplifier dissipates a lot of energy. In contrast, a switching amplifier has high energy efficiency, but the current ripple due to the switching degrades the current and positioning resolution of the system. Consequently, there is a design trade-off between the achievable precision and the energy efficiency.

As discussed in Section 1.2.2, GaN-based amplifiers have a potential to significantly increase the switching frequency of a switching amplifier. Because current or voltage ripples can be decreased by increasing the switching frequency there is a possibility to mitigate the precision vs. energy efficiency trade-off. However, there is a gap in research on applicability of high-frequency switching amplifiers, especially for a capacitive load such as a piezoelectric actuator in high-precision motion systems.

This thesis experimentally investigates a high-frequency switching amplifier that drives a piezoelectric actuator, which is regarded as a capacitive load, for possibility to improve the energy efficiency without degrading the precision of high-precision motion systems. Particularly, the influence of design parameters such as switching frequency on the energy efficiency, bandwidth and current ripple is evaluated in detail. The high-frequency switching amplifier for a piezoelectric actuator is also evaluated with an inductive load for comparison and better understanding.

1.3 Outline

Chapter 2 explains design principles and analyzes different design options. Each part of the developed system is explained in detail. Following the design, implementation and considerations taken into account during the implementation process are also

described in Chapter 2. Chapter 3 and 4 show experimental results when different load is attached to the output of the switching amplifier. In Chapter 3 experimental evaluation with coil is conducted and in Chapter 4 with piezoelectric actuator. All results are discussed and followed by theoretical explanations. Comparison of the results from Chapter 3 and 4 and final conclusion are given in Chapter 5, together with propositions for future research.

CHAPTER 2

System Design and Analysis

A system for driving piezoelectric actuator and evaluating its motions is considered. It consists of four parts as shown in Figure 2.1. Each part is separately designed in order to achieve high system performance.

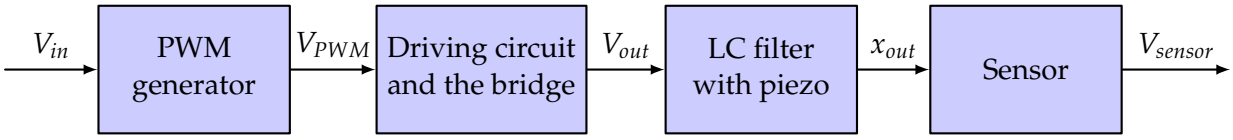

Figure 2.1: System diagram

Figure 2.2 shows the entire implemented system. All the system parts from the system diagram in Figure 2.1 are marked in Figure 2.2. The only difference is that the coil from LC-filter is soldered directly to the Printed Circuit Board (PCB) of the the gate driving circuit and the bridge, leaving the piezoelectric actuator a separate element. In the following sub-chapters component selection and integration of all named system parts is separately discussed.

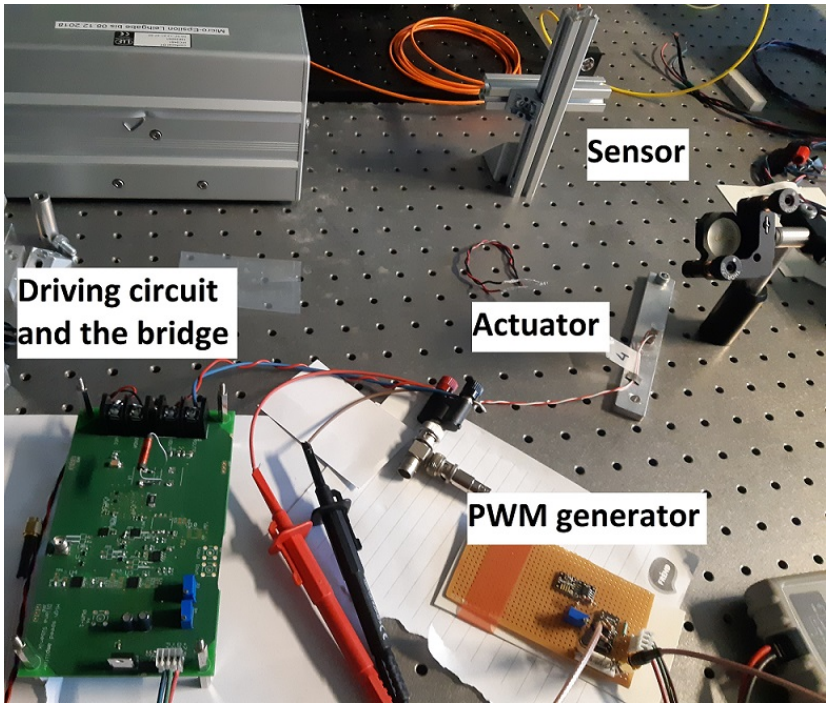

Figure 2.2: Implemented system

2.1 The Actuator

Piezoelectric actuator converts electrical signal to displacement in designed system. Piezoelectric actuators are made of special piezoelectric materials (e.g. quartz crystal) and they utilize piezoelectric effect exhibited by these materials for actuation [3]. Piezoelectric materials under compression generate an electric potential. This kind of behavior is called the direct piezoelectric effect. Opposite, if electric field is applied to the material it expands or contracts and this effect is called inverse piezoelectric effect. Since piezoelectric elements can be used as sensors, as well as actuators, they are called piezoelectric transducers.[3]

There are different types of piezoelectric actuators, and for the implemented system a piezoelectric stack actuator is selected. Piezo-stack actuators are multilayer actuators. To make a piezo-stack actuator, single piezoelectric actuators, which have electrodes on both sides are stacked and glued together to form a longer actuator. Stacking of multiple layers allows generating larger strokes with smaller actuation voltages. When a voltage V is applied on the actuator electrodes actuator displacement Δl is calculated by Equation (2.1). [3]

$$\Delta l = n \cdot h \cdot d_{33} \cdot \frac{V}{h} \tag{2.1}$$

Poling and actuation direction for the piezo-stack actuator is in the stacking direction, so piezoelectric coefficient for polarisation in that direction $d_{ij} = d_{33}$ is used. The number of layers n defines the length of an unloaded actuator, as well as positioning range of the stack-actuator. Length of an unloaded and unactuated actuator is calculated as the thickness of a single layer h multiplied n times plus the thickness of the

Table 2.1: Properties of selected piezoelectric actuator [26]

Attributes	Values
Length	14 mm
Operating voltage, max.	150 V
Free stroke, max.	19.8 µm
Capacitance	1080 nF
Blocking force, max.	1050 N

electrodes, glue lines and potentially a layer of unactuated ceramic material at both ends of the stack-actuator for isolation. [3]

Piezoelectric stack actuator is selected, because of its large stroke. Selected piezoelectric actuator *NAC*2013-*H*14-*A*01 (Noliac, DK-3490 Kvistgaard, Denmark) is of the same type as the one shown in the Figure 2.3.

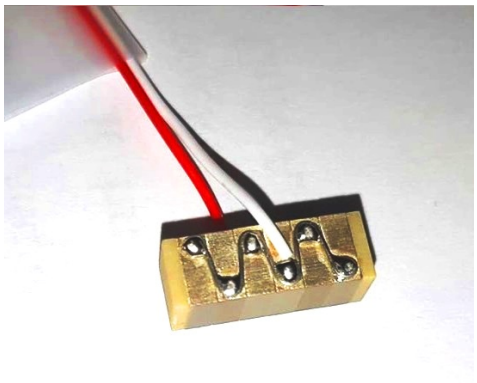

Figure 2.3: Piezoelectric actuator

Piezoelectric actuator converts electrical energy to mechanical energy and other way around, hence its mechanical and electrical properties need to be considered during the component selection process. Table 2.1 shows properties of the used piezo-stack actuator. Selected piezoelectric actuator has similar properties to piezoelectric actuators typically used in AFMs. The stroke of the selected actuator is 19.8 µm and it has mechanical resonance frequency at around 10 kHz. Since piezoelectric actuator is electrically modeled by a capacitor it can be used as part of the LC-filter.

2.2 The Position Sensor

To evaluate motion of the piezoelectric actuator its displacement needs to be measured. For the position sensor, an interferometer is selected, since it enables resolutions into the sub-nanometre region [3]. *IDS*3010 (attocube systems AG, 85540 Haar, Germany) is a fiber based low finesse Fabry-Pérot interferometer. Finesse is a

capability of interferometer to distinguish different wavelengths and it is determined by the ratio of reflection and transmission of the mirrors used in interferometer [3]. Interferometer $IDS3010$ measures absolute distance of the object and it operates within the absolute distance range 20 mm-1000 mm. Resolution and relative range depend on the protocol selected for reading out the measured data.

Interferometer used in the implemented system is $IDS3010$ Homodyne interferometer, where the term Homodyne refers to the use of light with only one frequency. The $IDS3010$ contains two different types of lasers. One infrared laser is used to perform displacement measurements. The second laser is the visible laser, which is used for setup alignment and is switched off for measurement operation. [27]

In Figure 2.2 the light path of the $IDS3010$ interferometer from the laser emitter to the actuator is visible. After the alingment procedure and setting the interference contrast signal to an appropriate value, it is necessary to choose output mode for the real-time position signal. AquadB Low-Voltage Transistor-Transistor-Logic (LVTTL) output mode is selected, because it quantizes the input signal and reduces the sensitivity to noise. This protocol transfers information about the relative measured position and position needs to be read out continuously as there is no information about the absolute value of the current position. Minimal resolution of this protocol is 1 pm . To use AquadB protocol, parameters *Resolution* and *Clock* need to be set, and the signal is then encoded over over two different 2-level-channels, A and B. Maximum velocity the AquadB protocol is determined through parameters *Resolution* and *Clock* and calculated by equation [27]:

$$\text{maximum velocity} = Resolution/Clock. \tag{2.2}$$

Clock parameter is chosen so that decoding of AquadB protocol can be done with FPGA. *Clock* is set to $80ns$ and *Resolution* to $200pm$ to achieve good performance. Maximum velocity that can be measured considering the chosen parameters is $2.5\,\mu m/ms$. This is sufficient to measure the response of piezoelectric actuators to input signals which have frequencies of few hundred Hertz and displacement range within 1 µm. FPGA is programmed to decode the AquadB (LVTTL) protocol in a way that one step in position change of ± 200 pm results in change of output voltage of FPGA for ± 1 mV.

2.3 The Amplifier

Switching power amplifier represents electronic part of the system that needs to be designed and developed. Switching power amplifier is specifically designed to drive the piezoelectric actuator introduced in Section 2.1. The switching power amplifier consists of four different parts, separately designed and implemented in the system. These four parts of switching power amplifier are shown in Figure 2.4. First part is the PWM generator shown as a comparator of input signal and triangular wave signal, which generates PWM signal on its output. This signal is used as an input to a gate driving circuit which represents the second stage. After PWM signal is

adapted to drive the Gates of the transistors, output stage transistors are switching and transferring the modulated input signal to a new output. This represents the third part of switching amplifier. The forth part is the LC-filter used for filtering of high frequency harmonics from a PWM signal. Piezoelectric actuator is used as a part of the LC-filter in switching power amplifier due to its electrical model.

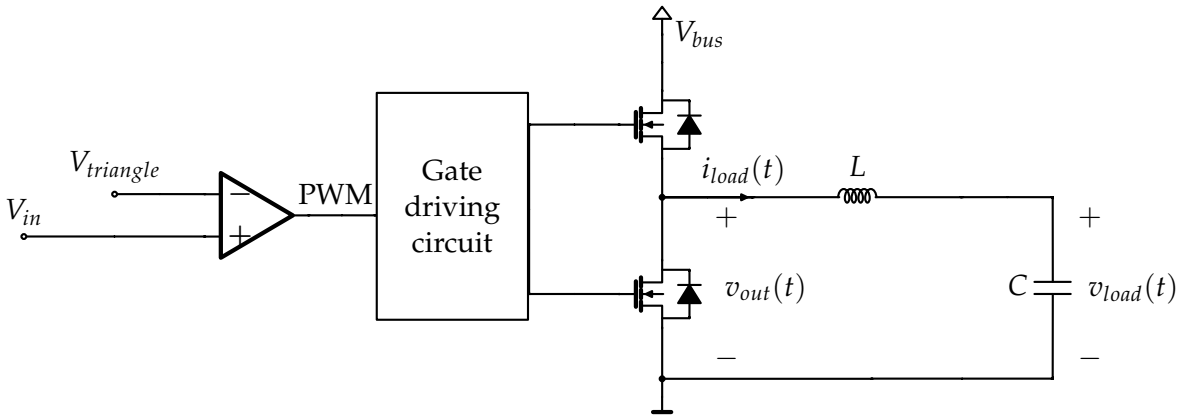

Figure 2.4: Diagram for the electrical part of the system

2.4 The Gate Driving Circuit and the Bridge

2.4.1 Bridge Design and Driver Selection

Parasitic Capacitance of FETs

Before explaining which components are selected for the half-bridge output stage it is important to introduce the main performance limiting factor of every switching transistor, the parasitic capacitance. Every FET has three parasitic capacitances. They are located between Drain and Source, Gate and Drain, and Gate and Source of the transistor. They are respectively named C_{ds}, C_{gd} and C_{gs}. These parasitic capacitances are main cause of reduction in energy efficiency of switching transistor with increasing switching frequency [11]. Parasitic capacitance determines the length of the switching transition, because they need to be charged or discharged during every transition. To describe the parasitic capacitance in terms of an effective input, output and reverse transfer capacitance, named C_{iss}, C_{oss} and C_{rss} respectively, an alternative system is given as follows:

$$C_{iss} = C_{gs} + C_{gd} \tag{2.3}$$

$$C_{oss} = C_{ds} + C_{gd} \tag{2.4}$$

$$C_{iss} = C_{gd}. \tag{2.5}$$

All the above described parasitic capacitances are nonlinear functions of Drain-Source voltage V_{DS}. This nonlinearity has as consequence that the charge stored in

parasitic capacitances is also a function of applied voltage [28]. Charge Q_{oss} stored in C_{oss} can be calculated with the following equation:

$$Q_{oss} = \int_0^{V_{DS}} C_{oss}(v)dv. \tag{2.6}$$

Power Dissipation of the Switching FET

Power dissipation in transistors can be divided in conduction losses and switching losses. Conduction losses can be calculated straightforward with the following equation:

$$P_d = R_{DS(on)} i_{load}, \tag{2.7}$$

where $R_{DS(on)}$ is the internal resistance of the transistor in ON state. Conduction losses, as the name says, occur only when transistor is in ON state conducting the current. Switching losses are related to transition of the switch from its ON state to its OFF state, and other way around. As switching frequency increases, number of transitions increases as well. That is why these losses are proportional to switching frequency and can be calculated by following equation:

$$P_{sw} = W_{tot} f_{sw}, \tag{2.8}$$

where W_{tot} is sum of all energy losses due to switching. Main switching losses occur due to charging and discharging of the parasitic capacitance C_{ds}, C_{gs} and C_{gd}. Parasitic capacitance output charge energy losses are given by the following equation [25]:

$$W_{Coss} = Q_{oss} V_{DS}. \tag{2.9}$$

Since the conduction losses depend only on duty cycle and $R_{DS(on)}$ which is very low in the FET ON state, they are negligible compared to switching losses in high frequency power amplifiers [29].

Selection of the Driver and the FET

Most important element of the switching power amplifier is a switching FET, because it determines maximum current and voltage values, that can be delivered to the load, together with output signal distortion. The GaN FET is selected so that it fulfills the requirements set by the selected piezoelectric actuator. Properties of piezoelectric actuator are given in Table 2.1. To excite the actuator, such that it can use the entire stroke range, it is necessary to provide output voltage of 150 V. For avoiding high current peaks, current to piezoelectric actuator is limited by a coil. Since current amplitude depends on different parameters, for flexibility reasons, it is decided to design the circuit which can provide ± 1 A current to the actuator.

Table 2.2 shows all major GaN-based components available in the market, that could be used for the given application. To achieve the desired high-frequency switching, all listed components can operate at switching frequencies of 1 MHz or more. 1 MHz is switching frequency 10 times larger than the switching frequency of typical MOSFET. Since piezoelectric actuator is a high voltage actuator, all the components

Table 2.2: GaN FET and driver selection

Component	Maximum voltage	Maximum current	$R_{DS(on)}$	C_{OSS}	Configuration
LMG5200	80 V_{pp}	10 A	15 mΩ	266 pF	Half bridge
LMG3410	600 V_{DS}	12 A	70 mΩ	71 pF	Single-Channel IC
EPC2112	200 V_{DS}	10 A	32 mΩ	150 pF	Single-Channel IC
EPC2007C	100 V_{DS}	6 A	24 mΩ	110 pF	FET
EPC2045	100 V_{DS}	16 A	5.6 mΩ	295 pF	FET
EPC2052	100 V_{DS}	8.2 A	10 mΩ	195 pF	FET
EPC2019	200 V_{DS}	8.5 A	36 mΩ	110 pF	FET
EPC2010C	200 V_{DS}	22 A	18 mΩ	240 pF	FET
EPC2012C	200 V_{DS}	5 A	70 mΩ	64 pF	FET
LM5113	80 V	1.2/5 A	–	–	Driver
LMG1205	80 V	1.2/5 A	–	–	Driver

in Table 2.2 can deliver high voltages. Not all listed might deliver 150 V, which means that depending on selected components, actuator will not be able to make use of the entire stroke range. This has as an advantage that more options are present in the list, and selection is more flexible. Listed components fulfill requirement to provide current of ±1 A to the actuator.

First step is to select a single FET component or a circuit where FET is already integrated with the driver. The advantage of selecting a separate FET and a driver component is in the experimental evaluation of signals in the circuit and power dissipation. In order to achieve highly efficient motion control, the parameter C_{oss} should be considered. As given by Equations (2.9) and (2.6), value of C_{oss} influences the energy losses caused by the switching. At high frequencies the main priority is to reduce switching losses [11]. Therefore it is important to choose FET with low C_{oss} parameter value. Considering all the requirements *EPC*2012*C* (Efficient Power Conversion Corporation, El Segundo, CA 90245,USA) is selected. For its driver it is important to prevent the gates of GaN FETs from exceeding the maximum Gate to Source voltage rating, because of their sensitivity to overshoot voltage. To fulfill those requirements, a half-bridge GaN driver *LMG*1205 (Texas Instruments Incorporated,Dallas, Texas 75243 USA) is most ideal. However, its package is DSBGA, which is difficult to manually solder due to its small size. Therefore, *LM*5113 (Texas Instruments Incorporated,Dallas, Texas 75243 USA) is selected instead.

Comparison of GaN FET with MOSFET

To clearly show its advantages, selected GaN FET is compared with a typical MOSFET. In Table 2.3 main parameters of MOSFET *IRFU*2407 and GaN FET *EPC*2012*C* are shown. The GaN FET has more than three times lower maximum Gate to Source, hence the GaN FET driver needs to be specially designed to prevent high voltage peaks of the Gate driving signal. Operating temperature is slightly higher for MOS-

Table 2.3: MOSFET and GaN FET parameters

Parameters	MOSFET IRFU2407	GaN FET EPC2012C
Maximum Gate to Source Voltage	±20 V	+6 V/-4 V
Operating Temperature	175 °C	150 °C
Gate Threshold	2 - 4 V	0.8 - 2.5 V
$R_{DS(on)}$	21.8 mΩ	70 mΩ
Switching Charge Q_G	74 nC	1 nC
Reverse Diode Recovery Charge Q_{RR}	400 nC	0 nC
Figure of Merit $R_{DS(on)}$ x Q_G	1613.2	70

FET, and GaN FET has lower threshold voltage. Q_G, which stands for the total Gate charge, is the amount of charge needed to charge Gate capacitance in order to turn *ON* the FET and Q_{RR}, meaning reverse recovery charge, is the charge accumulated in the FET body diode, when the diode is conducting. Q_G and Q_{RR} of GaN FET is significantly lower than of MOSFET, and as a consequence GaN FETs transition times are shorter. GaN FETs are switching faster and body diode does needs less time to stop conducting. $R_{DS(on)}$ is the value of resistance between Drain and Source, when transistor conducts current. Although $R_{DS(on)}$ of the MOSFET is lower than $R_{DS(on)}$ of the FET, lower FoM shows that GaN FET has better performance overall. Energy losses of GaN FET are reduced, due to the reduced charge stored in parasitic capacitance.

Bridge Design

As an output stage to drive piezoelectric actuator a half-bridge is used. Output stage of the switching power amplifier is shown in Figure 2.5. GaN FETs for the output stage and the driver to provide Gate signals *G*1 and *G*2 are selected, hence the rest of the the driving circuit is introduced in the following section.

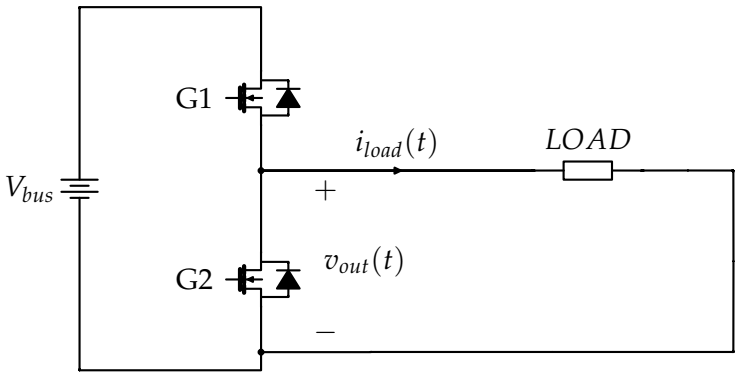

Figure 2.5: Half-bridge output stage

2.4.2 Logic and Dead-time Adjustment Design

Design of logic and dead-time adjustment circuit directly depends on selected GaN FET components. Gate driving circuit is shown in Figure 2.6. To generate gate driving signals, PWM signal is transformed. First, the dead-time is introduced, and afterwards signal is lead to logic circuits to make driving of both, high side by *HO* (high side gate drive output) and low side by *LO* (low side gate drive output) transistor possible. To drive the gates of the transistors the signals *HO* and *LO* are then lead to driver input. Since GaN technologies are used, the driver is selected accordingly.

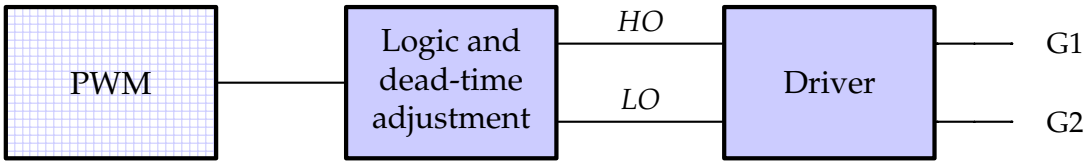

Figure 2.6: Gate driving signals

After other components are selected, the logic and dead-time adjustment circuit is designed. The dead-time needs to be introduced to avoid short circuiting the power supply when FETs are switching. When one FET is turning *ON* and the other one is turning *OFF*, a possibility that both FETs are turned *ON* has to be avoided because this could lead to overshoot currents and FET destruction. Trade-off needs to be made between having a too short dead-time, which might lead to short circuit, and too large output voltage distortion. To generate dead-time propagation delay *AND* logic circuit is used. The component used to generate dead-time is $SN74LVC08A$ (Texas Instruments Incorporated, Dallas, Texas 75243 USA) integrated circuit, that has four integrated *AND* logic circuits. Circuit design allows adapting dead-time, by using different number of *AND* logic, which is between one and four. Each *AND* logic has propagation delay of 2 ns for load capacitance of 50 pF, as given in the datasheet. All of the four *AND* logic are used, which results in 8 ns dead-time. The dead-time of a 5 ± 2 nanoseconds is sufficient for driving the GaN FETs [30]. This way the longest dead-time is achieved and therefore a probability of having nonoverlapping voltages is increased.

A and B are the inputs to the logical circuits *AND* (integrated component $74LVC1G08$ Nexperia, Nijmegen, Netherlands) and *NOR* (integrated component $74LVC1G02$, Nexperia, Nijmegen, Netherlands). As shown in Figure 2.7, dead-time circuit is connected between the PWM signal input and B input to the *AND* and *NOR* gates. When the PWM signal is high, meaning that A and B inputs to *AND* and *NOR* circuits are both high, an *HO* signal has high level, and an *LO* has low level. As soon as the PWM signal crosses threshold to reach low level, input A of *AND* circuit is registered as low, so the *HO* also falls to low level. During dead-time the *LO* signal stays at low level, and both FETs are turned *OFF*. Only after the output of the dead-time circuit also falls to low level the *LO* signal raises to high level. The same process is repeated after PWM signal raises to the high level again.

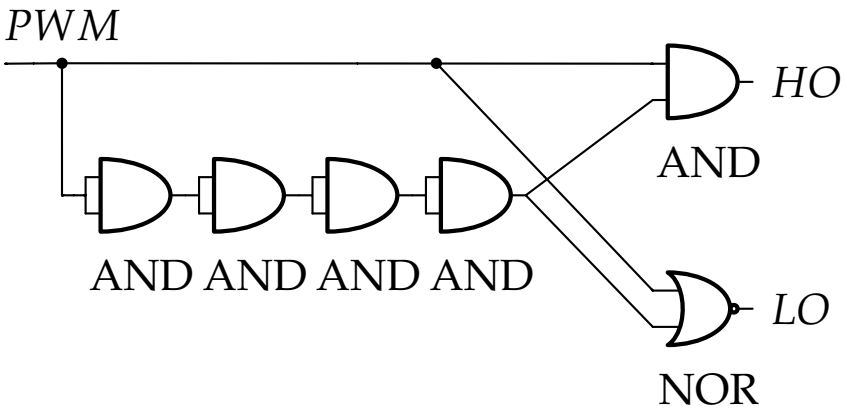

Figure 2.7: Logic and dead-time adjustment circuit

2.4.3 PCB Layout Design and EMI

EMI in Switching Power Amplifiers

Electromagnetic Interference (EMI) is one of the arising issues when switching power amplifiers are considered. As the switching frequency gets higher, EMI generated by switching power amplifier increases as well. High-frequency amplifier is a powerful EMI emitter because of the escalating frequencies involved. Transition times in high-frequency amplifiers range from a few nanoseconds to 100 nanoseconds. According to Maxwell's equations, a variation of electrical field with time produces a magnetic field, and opposite. This needs to be considered during the PCB design. Copper areas transferring swinging voltages and current loops containing high-frequency harmonics need to be minimized. Ground planes are also effective in reducing the EMI emissions. Emitted EMI needs to be in compliance with conducted and radiated emission limits.[11]

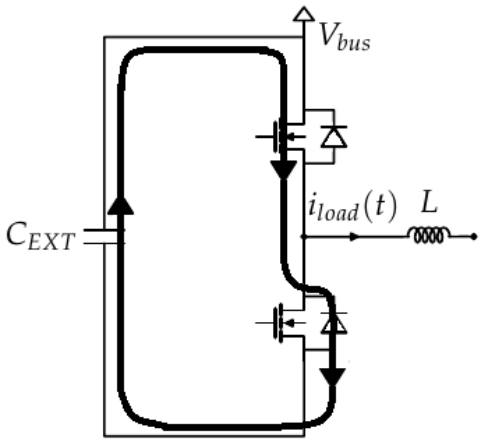

Figure 2.8: Half-bridge output stage for EMI analysis, drawn based on [31]

EMI in the class-D amplifiers comes partially from the reverse recovery current of the diode. To explain the process, amplifier circuit shown in the figure 2.8 is

analyzed. After switching off the lower transistor, diode starts conducting the output current during the dead-time. During this time the upper transistor is also turned off. After the upper transistor is turned on, the polarity of the voltage across the lower transistor is reversed. Since it was previously conducting current, the charge stored in the diode causes a fast and high short-circuit current as shown in Figure 2.8. Another cause of EMI in switching amplifiers is the switching of the output current. Power supply current is turned on and off by switching the upper transistor on and off. These effects can also be influenced and reduced during the amplifier design procedure. [31]

PCB Layout Design

Layout of the PCB is designed to avoid the EMI issues and parasites. Designed PCB is shown in Figure 2.9 and layout in Appendix A. Three bulk and decoupling capacitors, marked by (1) in Figure 2.9, used to smooth out the DC bus voltage variations and to filter the high frequency harmonics are added parallel to the V_{bus}. It is necessary to decouple the switching current from the power supply. Capacitors ensure that the half-bridge stage sees a low-impedance input voltage source at high frequencies. Voltage source $V_{cc} = 7.5\,\mathrm{V}$, marked with (2) in Figure 2.9, is used together with voltage regulator to power the driver and other integrated components used in the circuit. Same as for the V_{bus}, decoupling capacitors are needed to ensure that the high frequency harmonics are filtered. To achieve high performance it is important to take care of the parasites, such as leakage inductance. They are also related to the interconnections in the circuit, since they affect the switching behavior of the circuit [32]. Special attention needs to be provided to connections and components dealing with the switching current. For components, the Surface Mount Device (SMD) components without lead wires introducing self-inductance are selected [3]. The parasites of the two loops closing from two power supplies V_{bus} and V_{cc} are critical for the switching behavior [32]. That is why PCB is divided in two parts: left one where all high voltage components are placed, and right one where V_{cc} supply input and components that it supplies are placed. Since two layer PCB is used, bottom plane is used as ground plane. This way short current loops from the power supply to the component are closed. Additionally, around critical components, which are the FETs and the drivers, guard rings are placed to reduce parasitic interaction. All the connections transferring pulsating current are kept as short as possible and etch traps during routing circuit traces are avoided [33]. Special attention is given to design of the pads and traces around the $EPC2012C$ FETs, marked with (3) and circled by white ellipse in Figure 2.9. Because of their small size (pad size of 250 µm), the Ball Grid Array (BGA) routing guidelines are implemented [33]. Supply and ground solder pads of the FETs are connected through via to bottom layer, and the remaining gate driving pads use the top layer routing tracks.

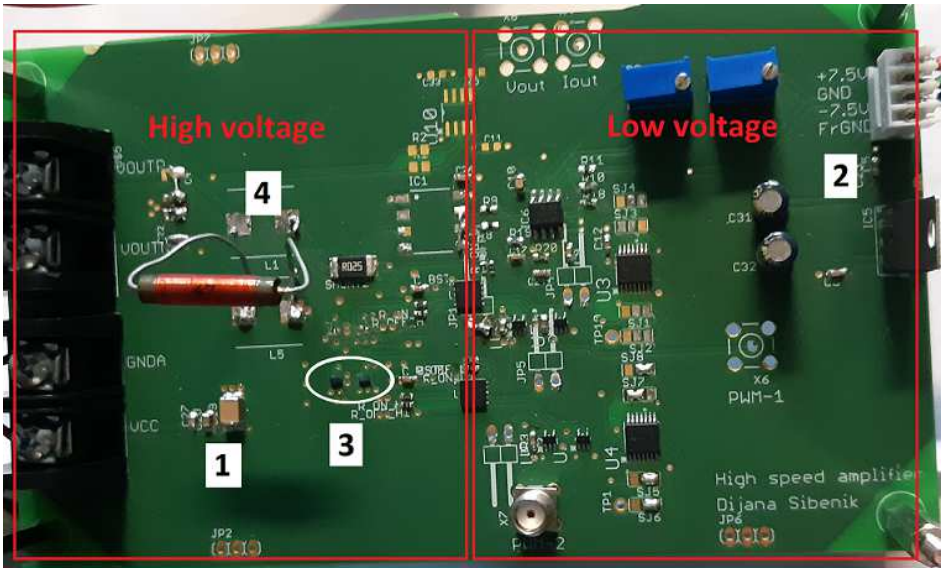

Figure 2.9: Implemented gate driving circuit and the bridge

2.4.4 Implementation of the Gate Driving Circuit and the Bridge

First step in the implementation process of high-frequency switching power amplifier is a layout development for the gate driving circuit and the bridge. *Autodesk EAGLE* software is used to draw PCB layout according to the layout design considerations from Section 2.4.3. After PCB layout is drawn, PCB is ordered for production. Together with the PCB stencil is ordered to make soldering of SMD components easier.

Figure 2.9 shows the implemented gate driving circuit and the bridge. Reflow oven is used to solder all the integrated circuit components. Stencil is used to add a solder paste on the produced PCB and the components are correctly positioned on their corresponding solder pads. When process is finished, PCB is put in the reflow oven, where all the integrated circuits are soldered. GaN FETs are components shown inside of the white ellipse in Figure 2.9. Since the GaN FETs are small, and their reflow profile differs from those of the typical integrated components and depends on the component density on the PCB [34], they are soldered manually. For soldering the GaN FETs a focused infrared light soldering system is used. To examine if FETs are properly soldered, Gate to Source and Drain to Source resistance is measured by a multimeter. Rest of the SMD components, capacitors and resistors, are also soldered manually. Because of their large number this procedure is easier than adding them on the PCB before reflow process. The last components which are soldered are the through hole components. For connection with power supplies and other system parts pin header, terminal blocks and SubMiniature version A (SMA) connectors are used. The pin header is used for the connection with low voltage power supply $V_{cc} = 7.5\,\mathrm{V}$, used for supplying the integrated circuits. Terminal blocks are used for the connection with high voltage input supply V_{bus}, and to transmit high voltage output signal to output load. To enable a low noise signal transfer, SMA connectors are used for receiving PWM input signal.

2.5 The PWM Generator

The input signal is first processed by a PWM generator. The PWM generator compares the input signal with a triangular signal to generate gate driving PWM signal for the transistors in the output stage. General idea is to drive the output stage transistors with the PWM signal which has frequency up to 1 MHz. Maximum switching frequency is limited by the selected driver, which can be driven with switching frequencies up to a few MHz. To achieve such a high switching frequency the PWM generator is built with components selected specially to meet these requirements.

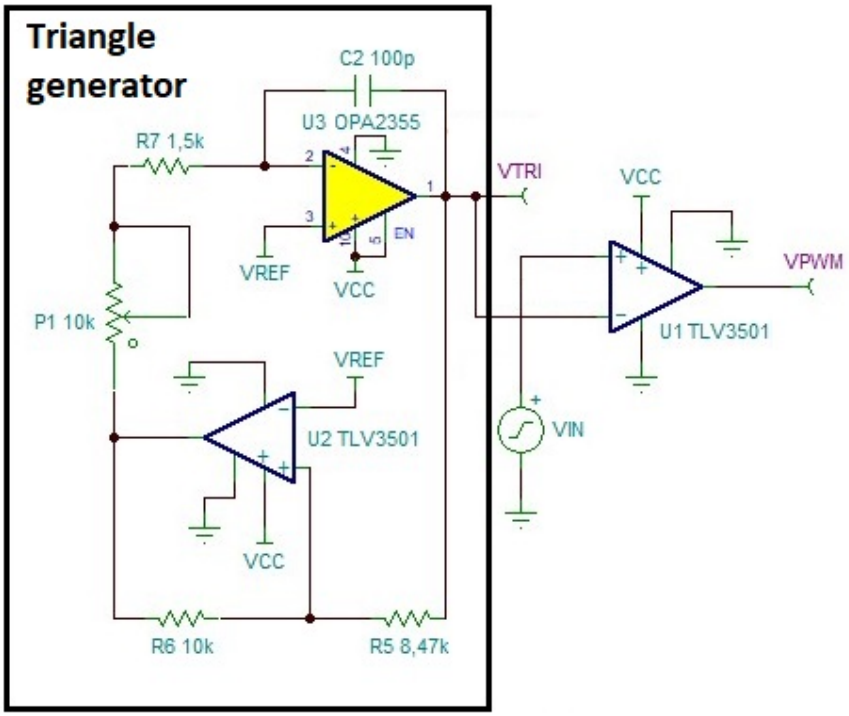

Figure 2.10: Simulation schematic for PWM generator circuit

Figure 2.10 shows a diagram of the designed PWM circuit. The output comparator U_1 compares the generated triangle wave signal V_{TRI} with the input signal to generate modulated signal V_{PWM}. When V_{TRI} is larger than V_{IN} the output of the comparator is 0 V, and when V_{IN} is larger the output of the comparator is high and equals comparator power supply voltage [35].

Components U_2 and U_3, representing comparator and operational amplifier respectively, are needed to generate the triangle wave. The operational amplifier works as an integrator. The output of the amplifier increases linearly when the output of the comparator U_2 is low, and opposite, decreases when the output of the comparator U_2 is high. The comparator U_2 output changes state when the voltage at its positive input passes the reference voltage $V_{REF} = 2.5$ V. Reference voltage is selected to be $V_{REF} = 2.5$ V because comparator is supplied by a 5 V power supply, which defines the high output voltage level. Values of resistors R_5 and R_6 determine the amplitude of the output triangle wave signal. The values are chosen so that the amplitude of V_{TRI} changes from 0.5 V to 4.5 V. The frequency at which the triangle

generator circuit oscillates and hence, the switching frequency of the output PWM signal is calculated from the following equation [35]:

$$f_{sw} = \frac{R_6}{4R_7R_5C_3}. \tag{2.10}$$

Selecting $C_3 = 100\,\text{pF}$ allows choosing R_7 as series connection of $10\,\text{k}\Omega$ potentiometer and $1.5\,\text{k}\Omega$ resistor. This way a PWM signal with switching frequency from 225 kHz to more than 1 MHz can be generated and transistors in the half-bridge output stage can be driven with different switching frequencies. The operational amplifier needs to have sufficiently high bandwidth and slew rate to be able to generate such high frequency triangle wave signal. Slew rate of the triangle wave is:

$$\text{slew rate} = 2 \cdot 4.5V \cdot 1MHz = 9\,\text{V}/\mu\text{s} \tag{2.11}$$

Taken that the minimum of 10 harmonics needs to be transferred to create a triangular wave [35] it can be determined that the bandwidth of the operational amplifier has to be 19 times larger than the frequency of the triangle wave. 10th harmonic of a triangle wave has frequency which is 19 times the fundamental wave frequency.

$$\text{bandwidth} = 19 \cdot 1MHz = 19MHz \tag{2.12}$$

To satisfy these requirements, an operational amplifier $OPA2355$ (Texas Instruments Incorporated, Dallas, Texas 75243 USA) is selected with 200 MHz bandwidth and $300\,\text{V}/\mu\text{s}$ slew rate. The used comparator needs to have a push-pull output topology to achieve fast and equal rise and fall times of the output signal without an excess power dissipation [35]. For a proper operation of the triangle wave generator and real time control of the output current or voltage, the comparator propagation delay needs to be much smaller than the period of PWM signal [35].

To fulfill the requirements $TLV3502$ (Texas Instruments Incorporated, Dallas, Texas 75243 USA) is used, as it has push-pull output topology and a typical propagation delay of 4.5 ns.

2.5.1 PWM Generator Implementation

The PWM generator circuit needs to enable driving of the output load with different input signal waveforms. For implementing a PWM generator circuit a stripboard is used. Implemented circuit is shown in Figure 2.11. Since integrated components used to generate a high frequency PWM signal are SMD components, Integrated Circuit (IC) base adapters are used to make soldering to stripboard possible. Pin headers are connecting the circuit with a voltage power supply, used for supplying the integrated circuits and providing reference voltage V_{REF}. In the first attempt, the pin header is also used for receiving the input signal from oscilloscope and transferring the PWM signal to the gate driving circuit input. This type of connection produces large noise and, sockets are not recommended for high speed amplifiers in general [36]. Instead, the SMA connectors are used for receiving the input signal from oscilloscope and transferring the PWM signal to the gate driving circuit input.

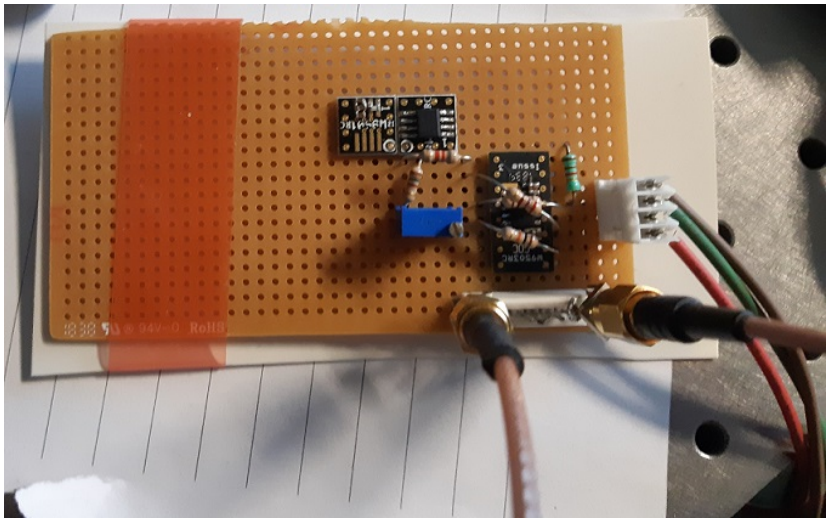

Figure 2.11: Implemented PWM generator

After testing the implemented circuit it is noticed that there is a problem with chattering of the output PWM signal. This issue is resolved by introducing hysteresis to the output comparator. Hysteresis for $TLV3501$ is calculated as [37]

$$V_{HYST} = V_+ \cdot \frac{R_1}{R_1 + R_2} + 6\,\text{mV}, \tag{2.13}$$

where V_+ is the value of voltage on the positive input of the comparator. Resistance values are chosen experimentally as $R_1 = 1.1\,\text{k}\Omega$ and $R_2 = 10\,\text{k}\Omega$, to avoid chattering. Schematic of the comparator with introduced hysteresis is shown in Figure 2.12.

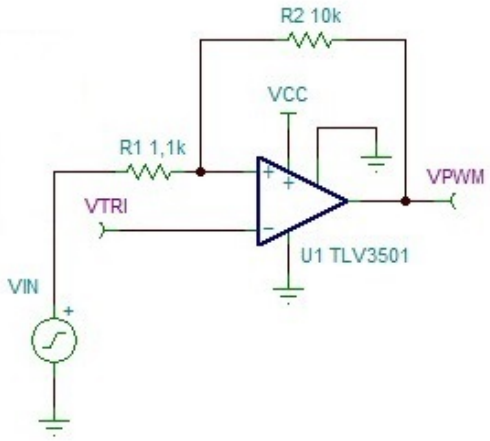

Figure 2.12: Simulation schematic for comparator with hysteresis

Table 2.4: Measured capacitance and series resistance values of piezoelectric actuator

Frequency	Capacitance	Resistance
10kHz	$C = 1.112\,\mu F$	$402\,m\Omega$
13kHz	$C = 1.069\,\mu F$	$984.7\,m\Omega$
15kHz	$C = 1.06\,\mu F$	$322.3\,m\Omega$

2.6 The LC-filter

To the output of half-bridge output stage, LC-filter is attached. As shown in Figure 2.13, the LC-filter is used to filter high frequency harmonics in the PWM output signal v_{out}. The output signal v_{load} of the LC-filter is shown in Figure 2.13. Only half-bridge is needed to drive the piezoelectric actuator, because piezoelectric actuator is driven only by a positive voltage. Hence the LC-filter is designed for the half-bridge output stage.

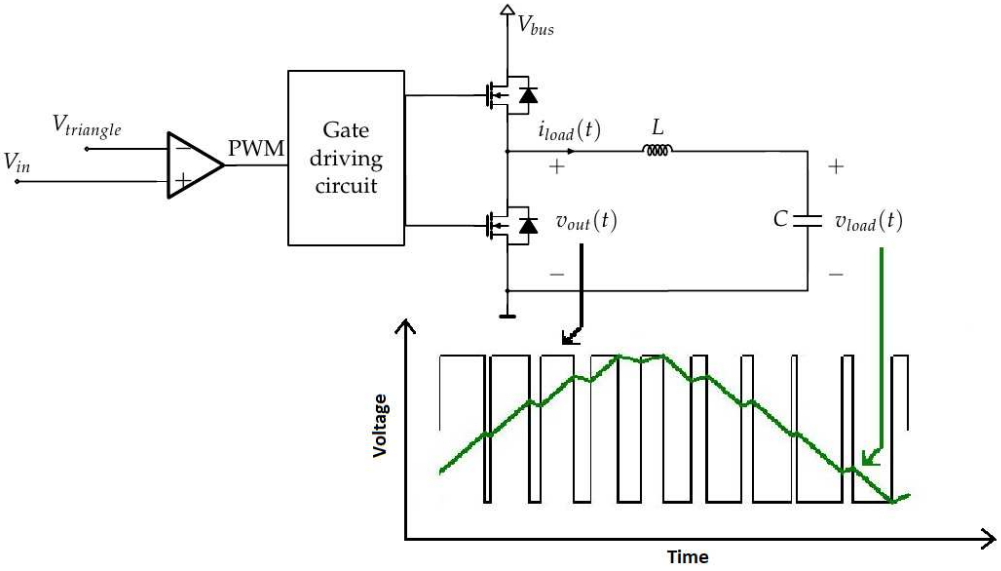

Figure 2.13: Low-pass filter input and output signals

As mentioned in Section 2.1, the piezoelectric actuator can be used as a part of the LC-filter. Capacitance and series resistance values of the selected piezoelectric actuator for different frequencies are given in Table 2.4, where the frequencies around mechanical resonance and anti resonance are the frequencies of interest. When an external voltage is applied to the piezoelectric actuator, the capacitance of the actuator is charged with a charge q which causes a displacement Δl [3].

Because of the electromechanical coupling, the mechanical properties of piezoelectric actuator have to be taken into account when designing a mechatronic positioning system [3]. Piezoelectric actuators have mostly high stiffness, so their mechanical resonances are high. With network analyzer it is determined that the piezoelectric

actuator has the mechanical resonance frequency f_r around 10 kHz. To use the maximum positioning bandwidth, the resonant frequency of the LC-filter needs to be set higher than f_r [38], but not too high, because high damping for high frequency harmonics is desirable.

The inductance of LC-filter is selected, such that the previously mentioned conditions are satisfied. For the inductance selected as $L = 47\,\mu H$ electrical resonance is set to 22 kHz. This is sufficiently higher than mechanical resonance frequency, but still large enough to significantly damp high frequency harmonics in the PWM output signal v_{out}. Since the capacitor and the inductor are reactive impedances in an electronic system, designed filter is second order low pass filter.

Inductor of the LC-filter is soldered to the developed PCB and is marked with (4) in Figure 2.9. Piezo-stack actuator used in the system and integrated in the LC-filter is shown in the Figure 2.14. Piezoelectric actuator is first glued to metal plate for stabilization reasons. Afterwards, mirror is added on the top of the actuator, such that the signal from the position measurement sensor can be reflected. Finally, the piezoelectric actuator is connected to the output of the PCB by a terminal block.

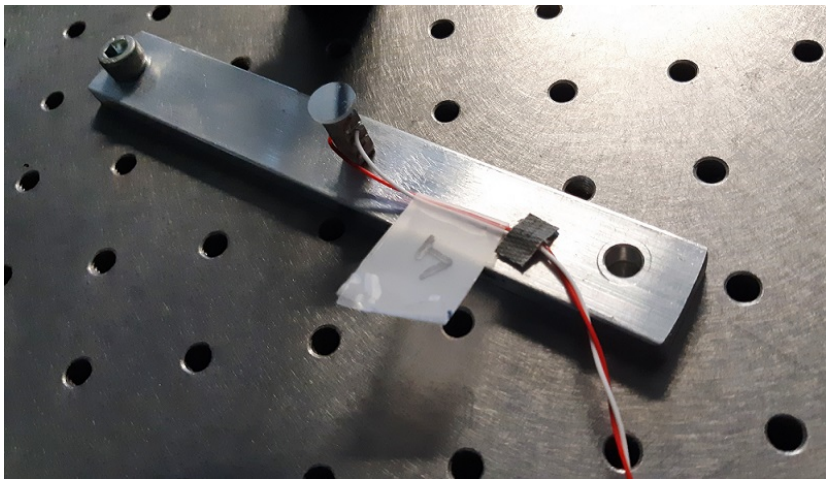

Figure 2.14: Piezoelectric actuator

CHAPTER 3

Experimental Evaluation for Inductive Load

For validation and for the comparison with a piezoelectric actuator, the switching power amplifier is evaluated with coil as dummy load in this chapter. Experimental evaluation is done without the PWM generator circuit, because for driving a Lorentz actuator, bipolar signal needs to be provided on the bridge output, and this does not coincide with the implemented circuit. That is why coil is used only as a dummy load to investigate the gate driving circuit and the bridge performance. Selected coil has inductance of $L = 24.76\,\text{mH}$ and resistance $R = 24\,\Omega$. Since the PWM generator is not used, instead of the PWM signal the gate driving circuit is driven by a square signal directly from the oscilloscope. By changing the duty cycle of the square signal and applying different bus voltages V_{bus}, different output currents can be generated. Half-bridge output stage with the dummy load is shown in Figure 3.1.

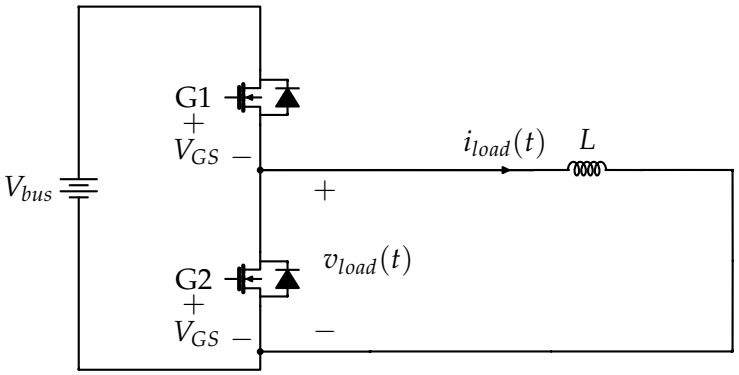

Figure 3.1: Half-bridge output stage with the dummy load

3.1 Half-Bridge Output Stage Signals

To evaluate the implemented circuit, gate driving signals V_{GS}, shown in the Figure 3.1, and circuit propagation delay are measured. From captured gate driving signals V_{GS} dead-time can be estimated. Dead-time is important parameter to consider for validating designed switching power amplifier.

3.1.1 Gate driving signals V_{GS}

When switching frequency is increased, the system used to measure the signals needs to satisfy certain requirements regarding system bandwidth. The bandwidth of the oscilloscope and the probe used for the measurement, must be high enough to correctly capture the fast change of the signals [32]. For correct dead-time measurement of GaN FETs, it is preferable to use probe with bandwidth of 250 MHz or more [39]. Figures 3.2 and 3.3 show gate driving signals V_{GS} of low and high side FET.

Signals in the Figure 3.2 are measured by *P*6100 (Jameco Electronics,Belmont, CA 94002, USA) probe with attenuation factor 10:1 and a 100 MHz bandwidth. Time difference between the moment V_{GS} of a low side FET starts falling and moment when V_{GS} of a high side FET starts rising represents dead-time. From Figure 3.2 dead-time is identified as 10 ns.

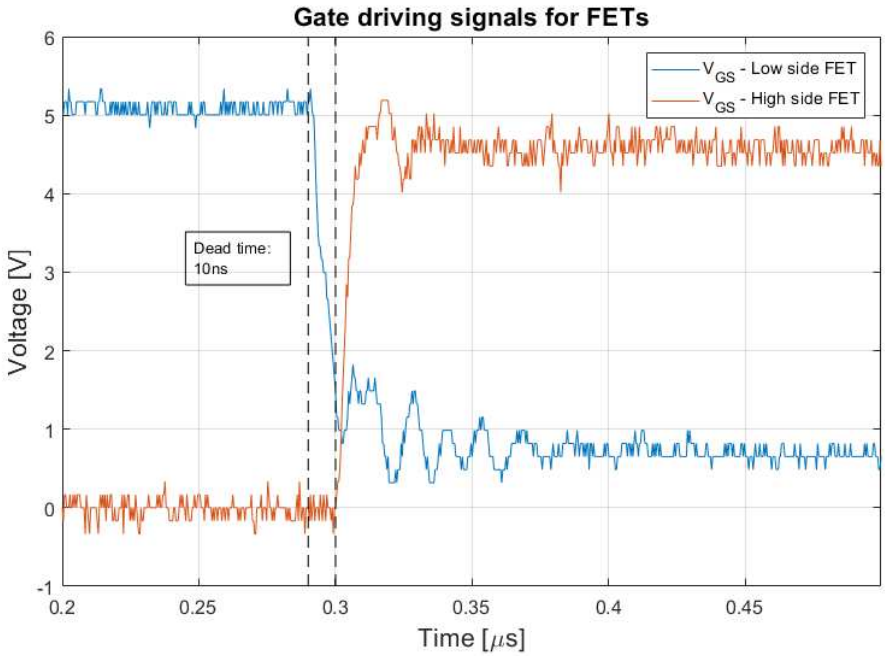

Figure 3.2: V_{GS} signals for high and low side FETs captured typical with passive probe

To capture signals in Figure 3.3 high bandwidth isolated probe is used. Probe is typically used to capture signals in GHz range. When comparing Figures 3.2 and 3.3, significant difference between the measured signals is visible. Dead-time measured from signals captured in Figure 3.3 is 7.5 ns. Identified dead-time corresponds to

dead-time calculated in Chapter 2.

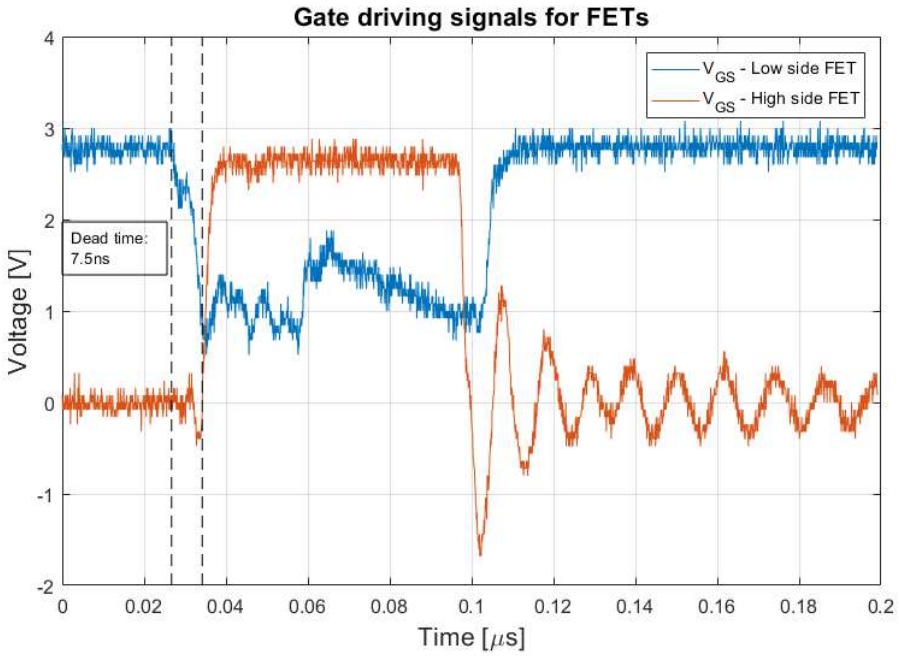

Figure 3.3: V_{GS} signals for high and low side FETs captured with isolated probe

3.1.2 Propagation Delay

Figure 3.4 shows propagation delay of output signal v_{out} to the PWM input signal shown in Figure 2.4. Signal v_{out} is measured by a voltage probe. Rising edge delay is 69.5 ns and it is larger from the falling edge delay which is 64 ns. This is consequence of the internal properties of integrated components used for dead-time adjustment and logic, and the driver, since they have different turn ON and turn OFF propagation delays. Propagation delay is important when considering system dynamics. Measured propagation delay is low, which means that it is possible to use the amplifier in a real-time feedback control loop.

GaN FETs have very fast response, because their parasitic capacitance is low. For the output voltage rising edge slew rate dV/dt is 1.86 V/ns, and falling edge slew rate is 1.47 V/ns. This allows shorter dead-times which then results in lower output voltage distortion.

3.1.3 Current Ripple

For high performance positioning system with an electromagnetic actuator it is important that an output signal on the load has low ripple. For that reason, ripple of the load current passing through the coil needs to be investigated. Current ripple

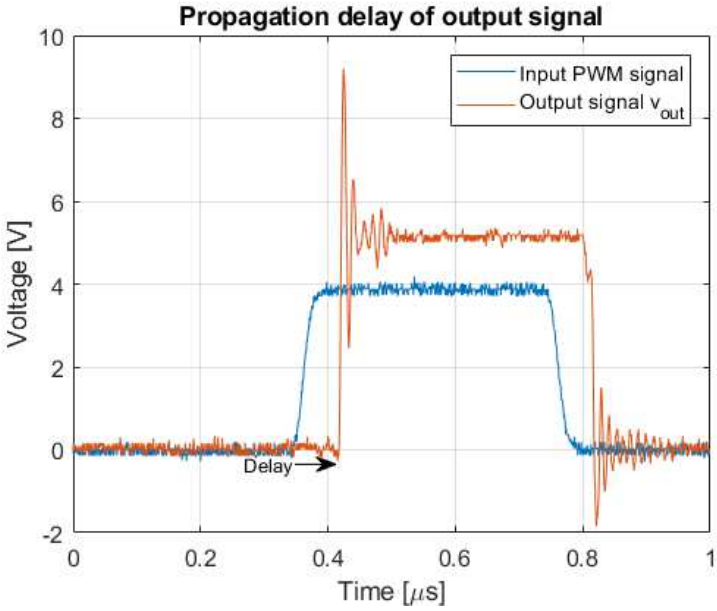

Figure 3.4: Propagation delay of input PWM signal to output signal v_{out}

can be calculated based on Ohm's law for inductor.

$$v_{load} = L\frac{di_{load}}{dt} \approx L\frac{\Delta i_{load}}{\Delta T}, \tag{3.1}$$

where $L = 24.76\,\text{mH}$ is the load inductance, v_{load} is voltage on the coil shown in Figure 3.1, i_{load} is current through the coil shown in Figure 3.1, and T is time period of one switching cycle. From this approximation, current ripple on the inductor attached to the output of the half-bridge is calculated as follows:

$$\Delta i_{load} = DV_{bus}\frac{1}{2Lf_{sw}}, \tag{3.2}$$

where D is the duty cycle, and f_{sw} is the switching frequency.

To measure current ripple current probe *Agilent* 1147*B* (Agilent Technologies, Santa Clara, CA 95051, USA) is used. Averaging is used to reduce the measurement noise of the current probe and AC coupling is set on the oscilloscope. Bus voltage on the amplifier output stage is $V_{bus} = 5\,\text{V}$ and the duty cycle length is $D = 0.2$. Figure 3.5 shows the load current i_{load} together with the input voltage from oscilloscope for different values of the switching frequency. For current ripple estimation, the load current value in the moment before the FET changes state is measured. At the moment when voltage v_{load} falls form high to low, or opposite, the load current should reach its highest or lowest value respectively. The lower value is subtracted from the higher one, and the result is divided by 2 to get the current ripple value. From Figure 3.5 it is visible that the current ripple at 20 kHz switching frequency is much larger than ripple at higher frequencies. Figure 3.17 shows an enlarged current signal at 1 MHz switching frequency. It is visible that current ripple is almost zero, but switching noise caused by discharging of parasitic capacitance is large.

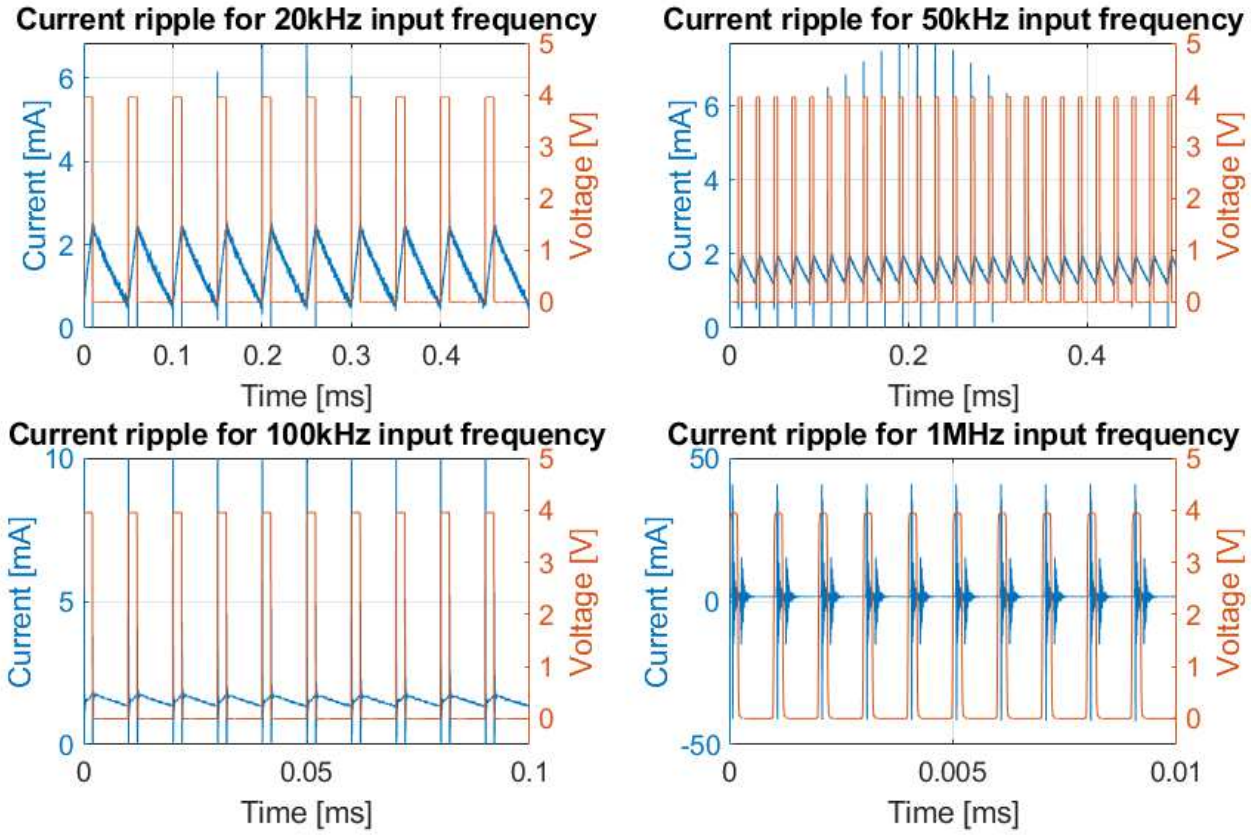

Figure 3.5: Current ripple

To analyze the current ripple measurement results Figure 3.6 is shown. Figure 3.6 shows how current ripple changes with increasing switching frequency. Experimentally measured current ripple values are shown and compared with values from the simulation and values calculated by the formula given in Equation (3.2). Experimental results are clearly validated by simulation and theory. All three approaches, experimental, simulation and theoretical one show that current ripple is reducing as switching frequency increases:

$$\Delta i_{load} \sim \frac{1}{f_{sw}}. \tag{3.3}$$

Overall, the experiments clearly show the benefits of high-frequency switching on decreasing the current ripple, since current ripple reduced 13 times by increasing frequency from 20 kHz to 1 MHz. Low current ripple is important for high resolution motion control.

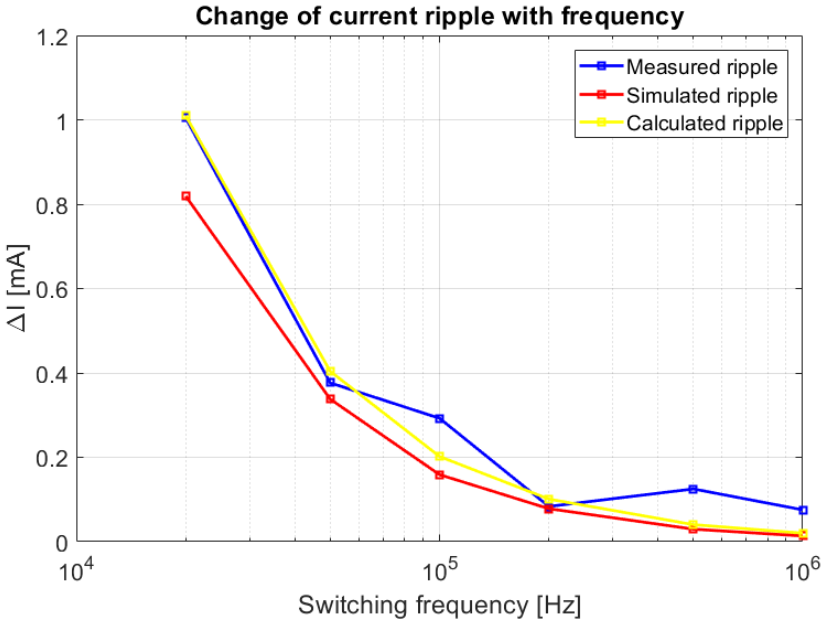

Figure 3.6: Resolution of the current ripple and the switching frequency

3.2 Power Dissipation

To evaluate efficiency of the high-frequency switching power amplifier, power dissipation is measured. The highest current and voltage are in the output stage of the switching power amplifier, thus power dissipation there is highest. Switching FETs are components transferring the high current and voltage, hence they are the main point of interest.

To retrieve information about the power dissipation from measured temperature, thermal resistance has to be introduced. Thermal resistance R_θ gives relationship between power dissipation in a component and its temperature rise. Value of thermal resistance depends on different factors, for example the geometry of the component. Mechanism by which heat is transferred from the component to the ambient is called convection. Convection is based on natural movement of air around the heated component. When heated, air expands and rises above cold one. [11]

Developed switching power amplifier uses only this natural convection principle to transfer heat to ambient. When device is turned on, temperature rises on the junctions between the components and the PCB. Most of heat is transferred from junction through thermal conduction to PCB and then from PCB to ambient by convection. Ground planes help in spreading the heat across the board and all exposed PCB surfaces help taking away heat by convection through air. Another heat transfer path exists, going from junction to component case and from case to ambient, but it has very high thermal resistance and it can be neglected. Thermal resistance between case and junction is low, so although measured temperatures are component case temperatures, due to the small temperature difference they are assumed as junction temperatures T_J. Dissipated power can be calculated from measured temperature

with following equation:

$$P_{loss} = \frac{T_J - T_{amb}}{R_{\theta JA}}, \tag{3.4}$$

where T_{amb} is the ambient temperature and $R_{\theta JA}$ is the thermal resistance for thermal dissipation from junction to ambient. Additional cooling systems such as fans and heat sinks can also be used to lower the temperatures. When a heat sink is mounted on the component power dissipation is calculated by equation:

$$P_{loss} = \frac{T_J - T_{amb}}{R_{\theta HA}}, \tag{3.5}$$

where $R_{\theta HA}$ represents thermal resistance for thermal dissipation from heat sink to ambient.

For measuring PCB temperature an infrared camera $FLIR\ E60bx$ (FLIR Systems, Wilsonville, USA) is used. To keep conduction losses constant during the measurement, bus voltage $V_{bus} = 5\,\text{V}$ and $I_{load} = 30\,\text{mA}$ are kept constant. Before capturing a thermal image and after setting all the parameters setup is left in idle state for 10 min to 15 min, in order to avoid all measurement errors due to thermal drift. Figure 3.7 - 3.10 show the temperature of the FETs and their driver, when different switching frequency is applied. In Figure 3.7 - 3.10 FETs are marked by a white ellipse and the driver by the black circle and $Sp1$ mark.

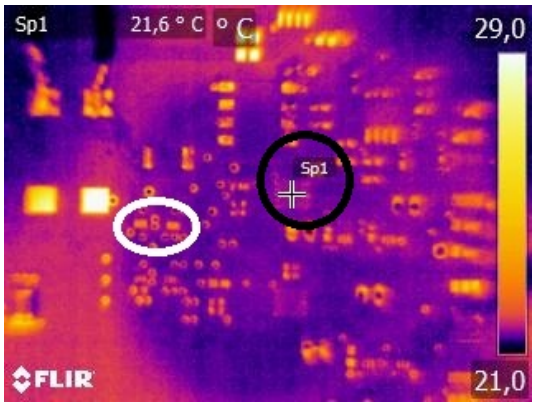

Figure 3.7: PCB temperature at 20 kHz switching frequency. GaN FETs are marked by a white ellipse, and the driver by the black circle.

Figure 3.8: PCB temperature at 100 kHz switching frequency. GaN FETs are marked by a white ellipse, and the driver by the black circle.

Based on the measured FET temperature in Figure 3.11 the relation with switching frequency is shown. FET temperature increases linearly with increasing switching frequency. Figure 3.12 shows diagram of the driver temperature. Driver temperature also increases in accordance with the switching frequency. It is to noticeable that the temperatures of both driver and the FET are constantly under 25 °C which is sufficiently lower than maximum operating temperature of the components of 150 °C.

As it is well captured by a linear trend lines in Figure 3.11 and 3.12, temperature of the FET and the driver increases linearly with increasing frequency, whereas

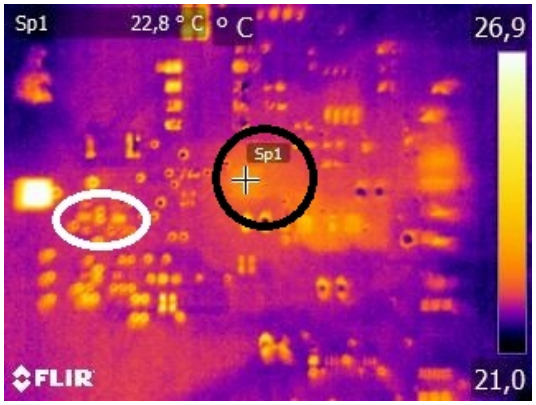

Figure 3.9: PCB temperature at 500 kHz switching frequency. GaN FETs are marked by a white ellipse, and the driver by the black circle.

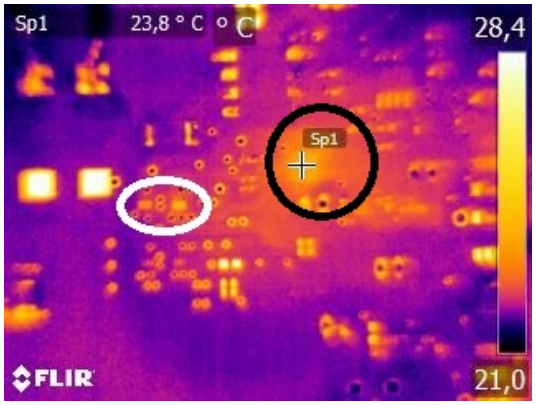

Figure 3.10: PCB temperature at 1 MHz switching frequency. GaN FETs are marked by a white ellipse, and the driver by the black circle.

the slope of the linear function is determined by sum of all energy losses due to switching, as shown in Equation (2.8). Since the temperature increases for less than 3 °C in switching frequency range of 20 kHz to 1 MHz, it can be stated that energy losses due to switching are low. Finally, it can be summarized that trade-off has to be made when increasing switching frequency, because current ripple is reducing, but temperature is increasing with increasing switching frequency.

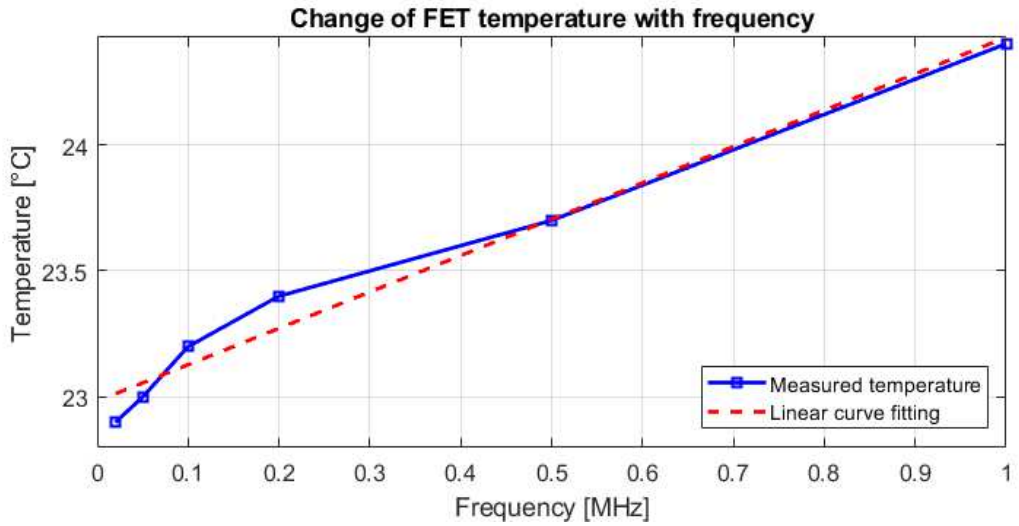

Figure 3.11: High side FET temperature increase with increasing switching frequency

Since coil usually needs to be supplied by high currents, measurement of temperature when $V_{bus} = 10\,\text{V}$ and $i_{load} = 200\,\text{mA}$ is conducted. Current is further increased and Figure 3.14 shows temperature measurement when $V_{bus} = 15\,\text{V}$ and $i_{load} = 400\,\text{mA}$. Switching frequency for both measurements is $f_{sw} = 1MHz$. $Sp1$ marks position of high side FET, $Sp2$ of the low side FET and $Sp3$ of the driver. Measured temperatures are shown in the Figures 3.13 and 3.14.

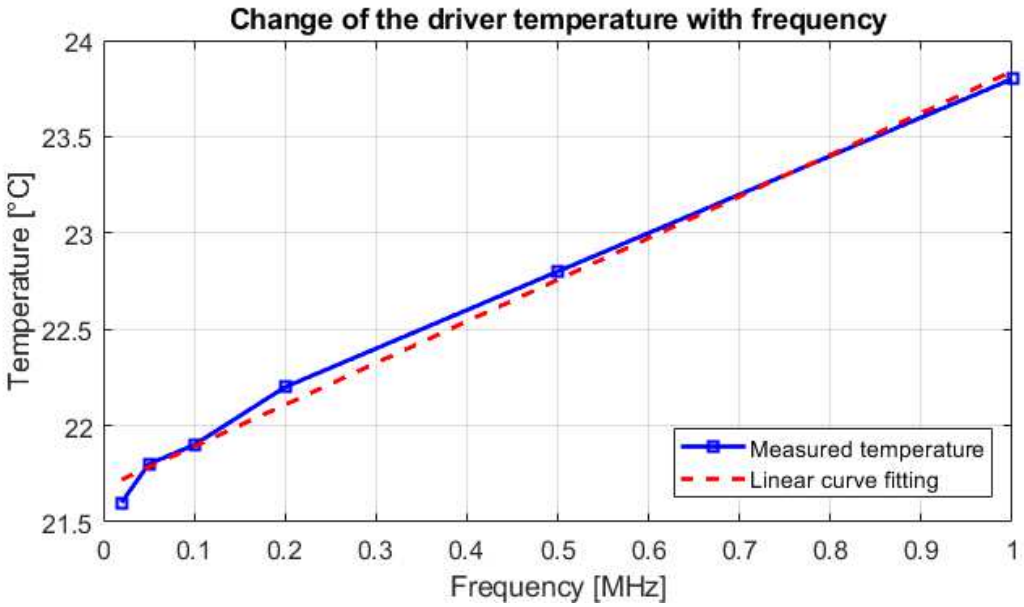

Figure 3.12: Driver temperature increase with increasing switching frequency

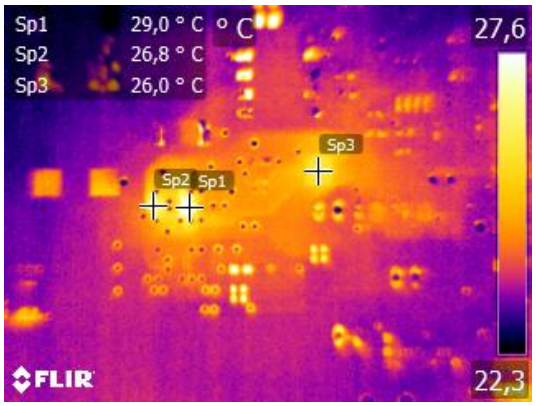

Figure 3.13: Measured temperatures for 200mA output current

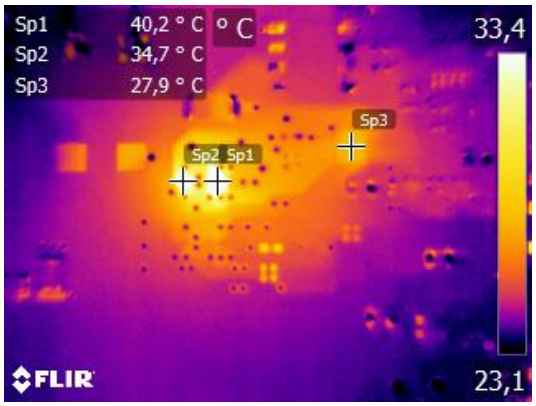

Figure 3.14: Measured temperatures for 400mA output current

Comparison of the developed GaN-based switching power amplifier with a linear power amplifier and a standard switching power amplifier described in [1] is presented. All three amplifiers are supplied by $V_{bus} = 15\,\text{V}$, and have an output load current $i_{load} = 400\,\text{mA}$. A standard switching power amplifier is driven at switching frequency of 10 kHz, and a GaN-based switching power amplifier at switching frequency of 1 MHz. Calculated power dissipation for different power amplifiers is given in Table 3.1 for ambient temperature $T_{amb} = 23\,^{\circ}\text{C}$.

Power dissipation of a GaN-based switching power amplifier is for an order of magnitude lower than the one of a standard switching power amplifier and more than 50 times lower than power dissipation of a linear power amplifier. Therefore, it can be stated that GaN-based switching power amplifier has much higher energy efficiency.

Table 3.1: Power dissipation comparison of different power amplifier amplifiers [1]

Amplifier type	Thermal resistance	Maximum temperature	Power dissipation
Linear	$R_{\theta HA} = 4\,^{\circ}\mathrm{C/W}$	68 °C	11.3 W
Switching - standard	$R_{\theta HA} = 5.6\,^{\circ}\mathrm{C/W}$	34 °C	2.0 W
Switching - GaN-based	$R_{\theta JA} = 85\,^{\circ}\mathrm{C/W}$	40.2 °C	0.2 W

3.3 Switching of GaN FET

For evaluating a high-frequency switching power amplifier, switching losses need to be considered, since they increase linearly with frequency. Switching losses arise due to dynamic processes in the transistor [3]. Dynamic processes are represented by current and voltage changes in the transistor, when it is changing its state from *ON* to *OFF*, and other way around. These current and voltage transients in the transistor are determined by the values of parasitic capacitance, load current and voltage values [40]. The dynamic processes can cause a new problem which arises over the switching transistors because of hard switching transients.

3.3.1 Analysis of Hard Switching of GaN FETs

Hard switching occurs when there is certain overlapping between the Gate and Drain rising and falling edges, as shown in the Figure 3.15 A. Hard switching happens when GaN FET is turned *ON* before all dynamic processes in transistor are over. This means that Gate to Source voltage increases over threshold voltage $V_{GS} > V_T$, before Drain to Source voltage V_{DS} falls to zero. When the FET is in the *OFF* state, voltage equal to bus voltage V_{bus} appears between Drain and Source. When the FET is turned *ON*, Drain to Source voltage V_{DS} has to rapidly drop from V_{bus} to almost zero, while the drain current I_D has to increase and become equal to the load current i_{load}, determined by the load inductor. This process is shown in Figure 3.16. Because of discharging process of the C_{oss} capacitance, current spike appears [42], [28]. During the transition period high current and high voltage are simultaneously present. Because the power loss is given by the product of the voltage and the current, hard switching results in a high energy loss for every switching action.

Soft switching event is shown in Figure 3.15 B. For soft switching, Drain voltage is already low when Gate voltage crosses the threshold. This results in a negligible drain current I_D and consequently power dissipation. [21]

Additionally, hard switching related to the conducting diode exists. When the load current i_{load} flows in the opposite direction through the FET which is turned *OFF*, the next device turn ON will always be hard switching and require reverse recovery of the conducting diode [40]. This process is described in Section 2.4.3. Body diode of GaN FET is just the channel conducting in reverse and a majority carrier operation [40]. Therefore reverse recovery time of the integrated diode is significantly reduced in GaN FET. Since GaN FETs have reverse recovery charge $Q_{RR} = 0$, there are no large hard-switching losses caused by conducting diode [18].

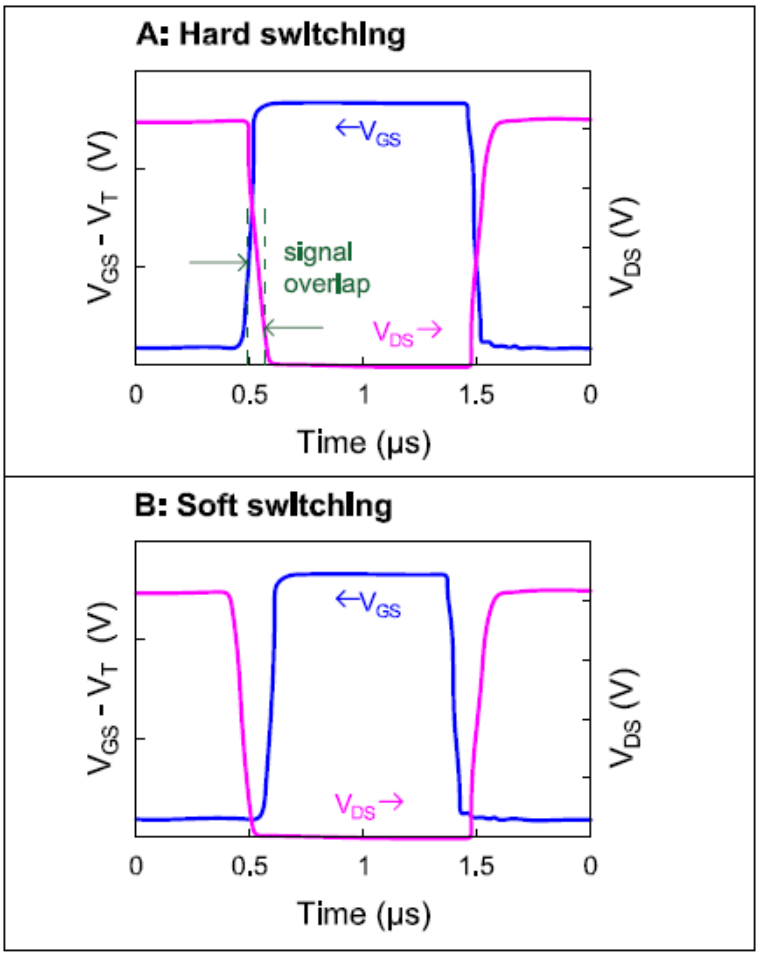

Figure 3.15: V_{GS} and V_{DS} waveforms for hard (A) and soft (B) switching, drawn based on [41]

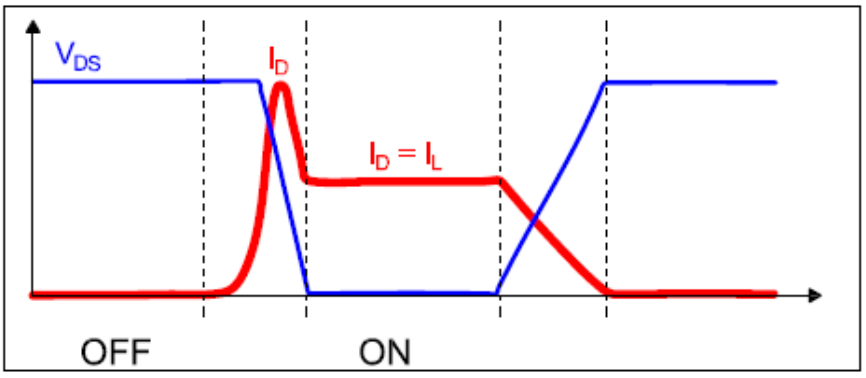

Figure 3.16: Representation of the waveforms of V_{DS} and I_D during a switching event, drawn based on [21]

Dead time should be optimized to minimize hard switching effect and reduce power losses [40].

3.3.2 Switching of Inductive Load

Because of the nonlinear characteristic of C_{oss}, which has to be taken in consideration in calculations and analysis, some significant values of C_{oss} for different voltages V_{DS} are given in Table 3.2.

To examine the switching process, output current i_{load} and voltage v_{load} are observed. Transfer function from input to output voltage of switching amplifier with inductive load is $\frac{V_{out}}{V_{in}} = 1$. This means that output voltage on the bridge equals voltage on the inductor. When FET is turned OFF, voltage on the bridge v_{load} changes very fast, forced by the current in the inductor that needs a voltage step to change [3]. Transfer function from output voltage to output current is given by the equation

$$\frac{i_{load}}{v_{load}} = \frac{1}{R + Ls}. \tag{3.6}$$

$L = 24.76\,\text{mH}$ is coil inductance and $R = 24\,\Omega$ and represents coil series resistance. According to energy conservation law, the current through the coil is mainly DC with some superimposed harmonics. This means that in the switching moment Equation (3.6) has theoretical value of $\frac{1}{R}$, because $s = 0$. Therefore when the parasitic capacitance starts discharging, it discharges over coil series resistance R. After high peak appears, transfer function from output voltage to output current is not $\frac{1}{R}$ anymore, but coil starts resonating with parasitic capacitance as shown in the Figure 3.17.

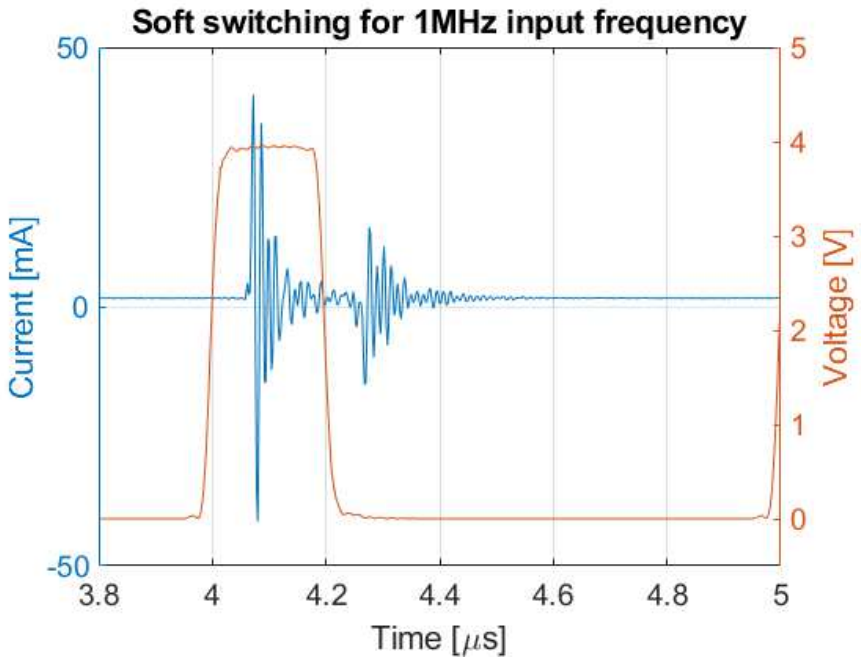

Figure 3.17: Soft switching and current ripple at 1MHz switching frequency

Transition processes in GaN FET when inductive load is attached to the output stage are described further. For calculation, values of $C_{oss}(V_{bus})$ are taken from Table 3.2. Switching event causes current through the parasitic capacitor between the

Table 3.2: Values of parasitic capacitance C_{oss} for different voltages V_{DS} [19]

V_{DS}	C_{oss}
0 V	210 pF
5 V	200 pF
20 V	150 pF
100 V	70 pF
200 V	50 pF

Drain and the Gate of the switching FET [3]. This current that keeps the FET conducting for a short time [3]. When parasitic capacitor starts discharging it dissipates energy over coil series resistance R_{load}. Parasitic capacitance will discharge with the time constant $\tau = R_{load}C_{oss}$, which will for $V_{bus} = 20\,\text{V}$ be

$$\tau = R_{load}C_{oss}(V_{bus}) = 24\,\Omega \cdot 150\,\text{pF} = 3.6ns. \tag{3.7}$$

This time constant is shorter than the dead-time, hence hard switching is not occurring with inductive load, and most of energy accumulated in parasitic capacitance is dissipated on the load, since coil series resistance is more than 100 times larger than internal FET resistance $R_{DS(on)}$.

Switching condition, meaning if switching transition in the transistor is hard or soft, can be checked by following equation [28]:

$$\frac{LI^2}{2} \geq Q_{oss}(V_{bus})V_{bus} \tag{3.8}$$

As a sufficiently good approximation of Equation (3.8) at low voltages, Equation (3.9) is used.

$$\frac{LI^2}{2} \geq C_{oss}(V_{bus})V_{bus}^2 \tag{3.9}$$

$$\frac{24.76\,\text{mH} \cdot 0.03^2\,\text{A}^2}{2} \geq 200\,\text{pF} \cdot 5^2\,\text{V}^2 \tag{3.10}$$

$$10.8\,\mu\text{J} \geq 5\,\text{nJ} \tag{3.11}$$

Since the Equation (3.8) is fulfilled, soft switching is achieved [28].

CHAPTER 4

Experimental Evaluation with Piezoelectric Actuator

To investigate the influence of a high-frequency switching on a piezoelectric actuator, the power amplifier developed in Chapter 2 is evaluted with the piezoelectric actuator in this chapter. Output stage together with the LC filter is shown in the Figure 4.1. PWM generator is used to drive the gates of FETs as described in Chapter 2. Different input signals are applied to the PWM generator (sine wave, triangular wave, DC signal) to measure different characteristics of the system. Interferometer is used to measure the position of the piezoelectric actuator, as described in Chapter 2.

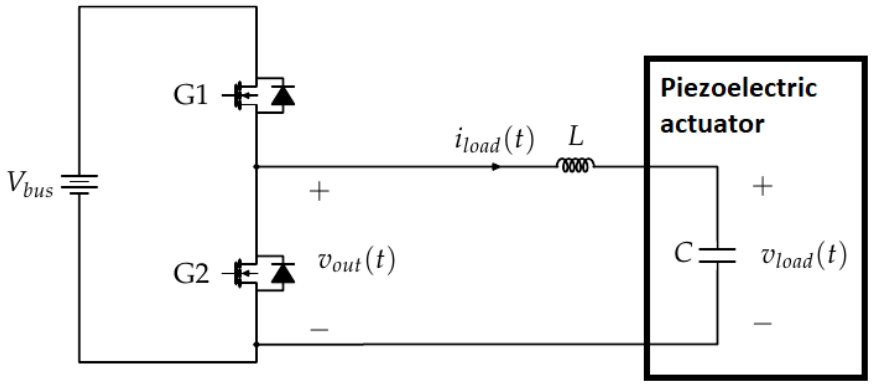

Figure 4.1: Switching power amplifier output stage with LC filter

4.1 Measured Bode-plots

In order to investigate the frequency response and the bandwidth, network analyzer is used to measure Bode-plots in this Section.

4.1.1 Bode-plots from Input Voltage to Output Voltage

Figure 4.2 and 4.3 show the measured Bode-plot from v_{in} to v_{out}, where v_{out} is voltage on the piezoelectric actuator v_{load} shown in the Figure 4.1. Different Root-Mean Square (RMS) levels of output voltage and of the transfer function gain are achieved by changing the bus voltage V_{bus} values on the output stage of the switching amplifier.

When the bus voltage of 20 V is applied, the electrical resonance peak in magnitude response is damped. The resonance can still be recognized in phase response, where phase reaches $-90°$ at 22 kHz. While reducing the bus voltage gradually, damping of the resonance peak reduces. After the bus voltage is reduced to $V_{bus} = 3$ V, it is possible to see a clear resonance peak of the LC-filter at 22 kHz. This is shown in Figure 4.3.

Reduction in a resonance peak visible in Figure 4.2 can be consequence of saturation or influenced by mechanical properties of the piezoelectric actuator. Electromechanical coupling is influenced by mechanical modes of the mirror which is attached to the top of the piezoelectric actuator. The measured resonance in both figures matches the one calculated in Chapter 2. Measured bandwidth is sufficiently higher than the mechanical resonance of piezoelectric actuator at around 10 kHz, whereas switching frequency harmonics for high switching frequency are well damped.

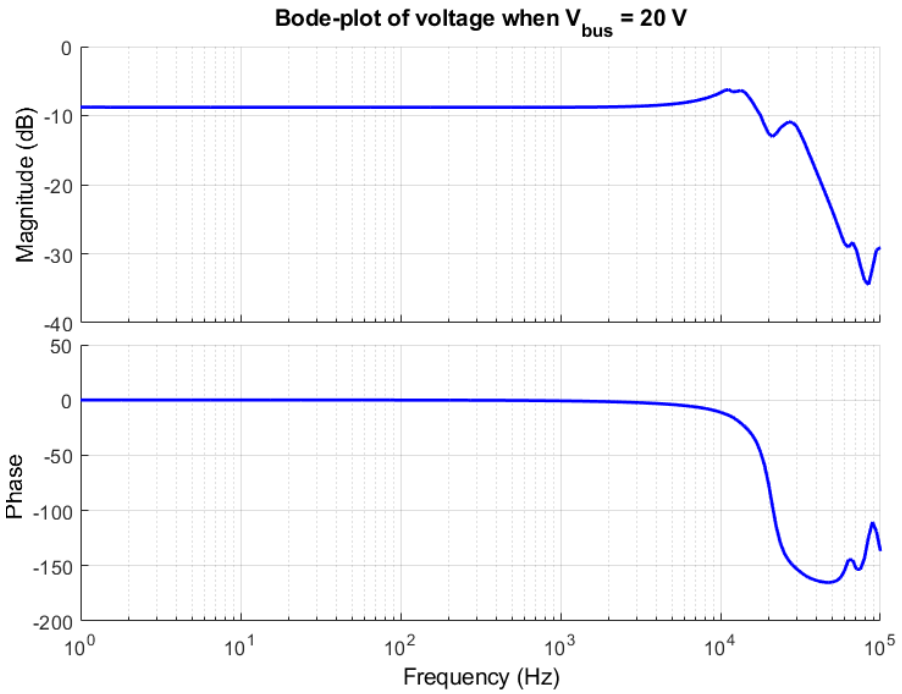

Figure 4.2: Bode-plot with the bus voltage 20V

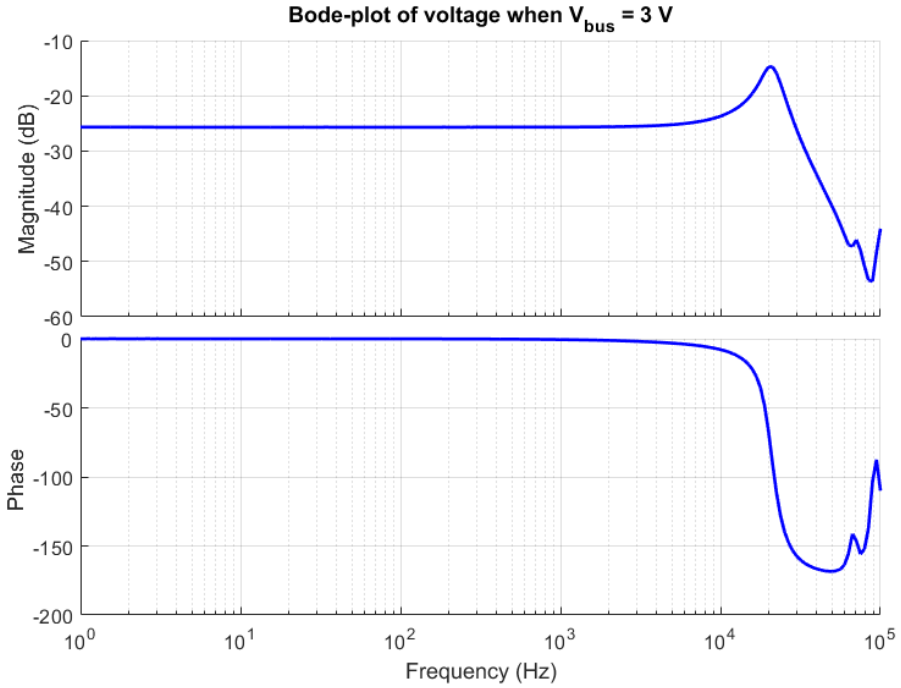

Figure 4.3: Bode-plot with the bus voltage 3V

4.1.2 Bode-plots from Input Voltage to Piezoelectric Actuator Position

To evaluate the influence of the power amplifier on motion control, a Bode-plot from the amplifier voltage input v_{in} to the actuator position x_{out} is measured. First, switching power amplifier with a low bus voltage is used for driving the piezoelectric actuator, because of the effects of mechanical coupling or saturation. Figure 4.4 shows the system transfer function when $V_{bus} = 1\,\text{V}$. This Bode-plot includes mechanical properties of the system. It is visible that the mechanical resonance peak occurs at 6 kHz and it is followed by anti resonance at 9 kHz. Additionally, electrical resonance at 22 kHz is visible, as shown in Figure 4.3. From the phase diagram in Figure 4.4 it is visible that time delay is present in the system. Time delay is measured to be around 17 µs. Analysis has shown that time delay is caused by digital processing units in the circuit, as well as hysteresis introduced in PWM generator to prevent the chattering, as described in Section 2.5.1.

Figure 4.5 shows system response when $V_{bus} = 10\,\text{V}$ is voltage on the output stage of the switching amplifier. The resonance peak at 6 kHz, which corresponds to mechanical resonance of the piezoelectric actuator, is well damped at this bus voltage level. The electrical resonance of the LC-filter is still visible in phase diagram.

LC-filter on the output of the switching power amplifier needs to eliminate high switching frequency harmonics without significantly influencing the ground frequency signal. This limits the bandwidth of switching power amplifier to approximately 10% of the switching frequency, so that the unwanted ripples are sufficiently filtered. Therefore, switching power amplifiers have to make compromise between output filter resonance frequency, switching and signal ground frequency. Previously,

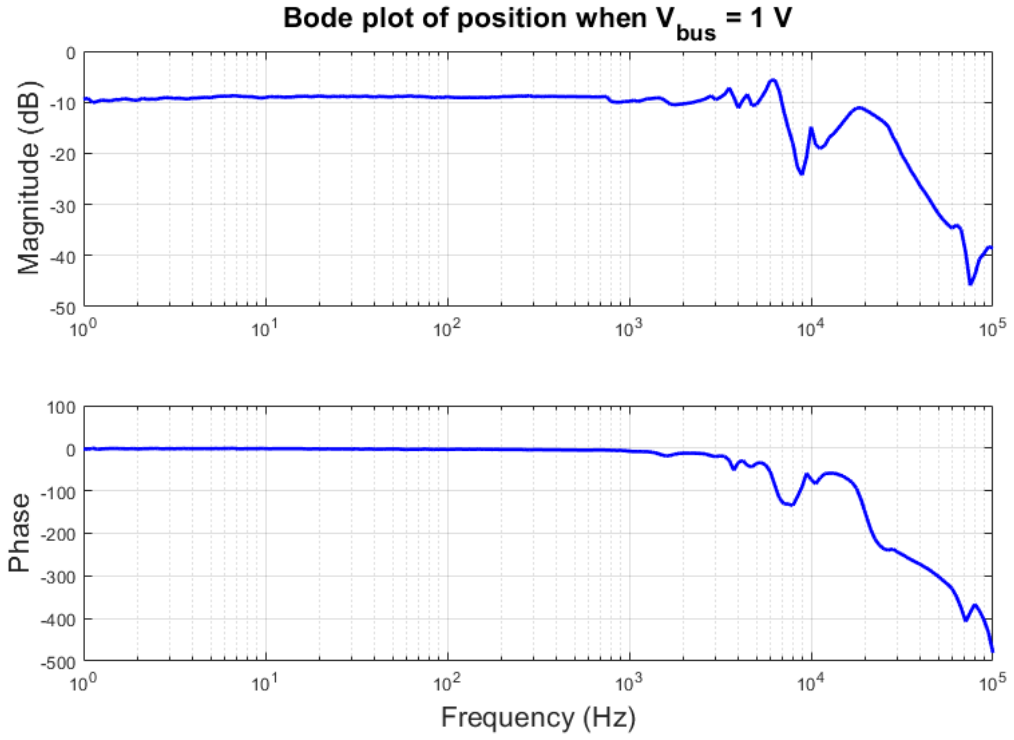

Figure 4.4: Bode-plot of position with switching amplifier when $V_{bus} = 1V$

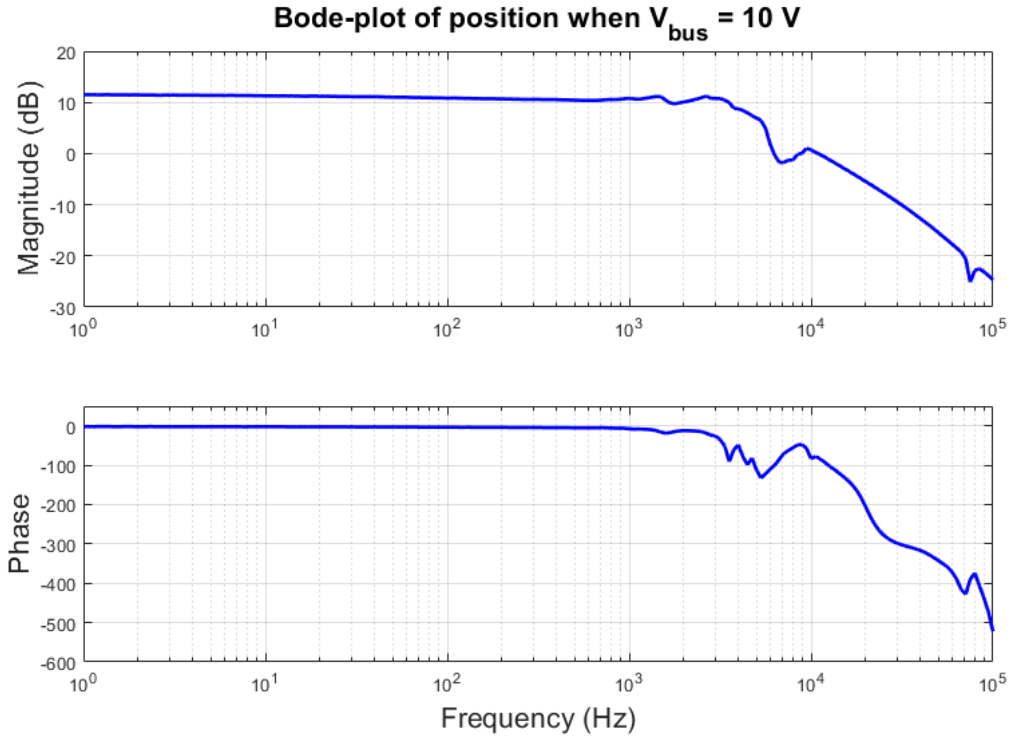

Figure 4.5: Bode-plot of position with switching amplifier when $V_{bus} = 10V$

this caused that switching power amplifiers have smaller bandwidth in comparison

to the linear ones. [17]

The bandwidth of the switching power amplifier with piezoelectric actuator is limited by mechanical resonance at 6 kHz. Electrical resonance at 22 kHz sets requirement on the switching frequency, to be approximately 10 times higher, which means switching frequency of 220 kHz or more. This is achievable with high-frequency switching power amplifier.

For comparison, Figure 4.6 is given and it shows transfer function when linear power amplifier *Falco Systems WMA-300 High Voltage Amplifier DC-5MHz* (Falco Systems BV, Katwijk aan Zee, Netherlands) is used for driving the piezoelectric actuator. The amplitude of the output voltage delivered to piezoelectric actuator from linear amplifier is 2 V. From comparison of Figure 4.4 with Figure 4.6 is visible that bandwidth of the developed switching power amplifier is higher than the bandwidth of the linear power amplifier, which is only 1 kHz. Used linear power amplifier is specially designed to be used for different demanding applications including piezoelectric actuator based positioning systems. Since bandwidth of the linear power amplifier is dependent of the capacitance of piezoelectric load, for 1.1 µF capacitive load it is significantly reduced. It can be stated that high-frequency switching power amplifier increases system bandwidth.

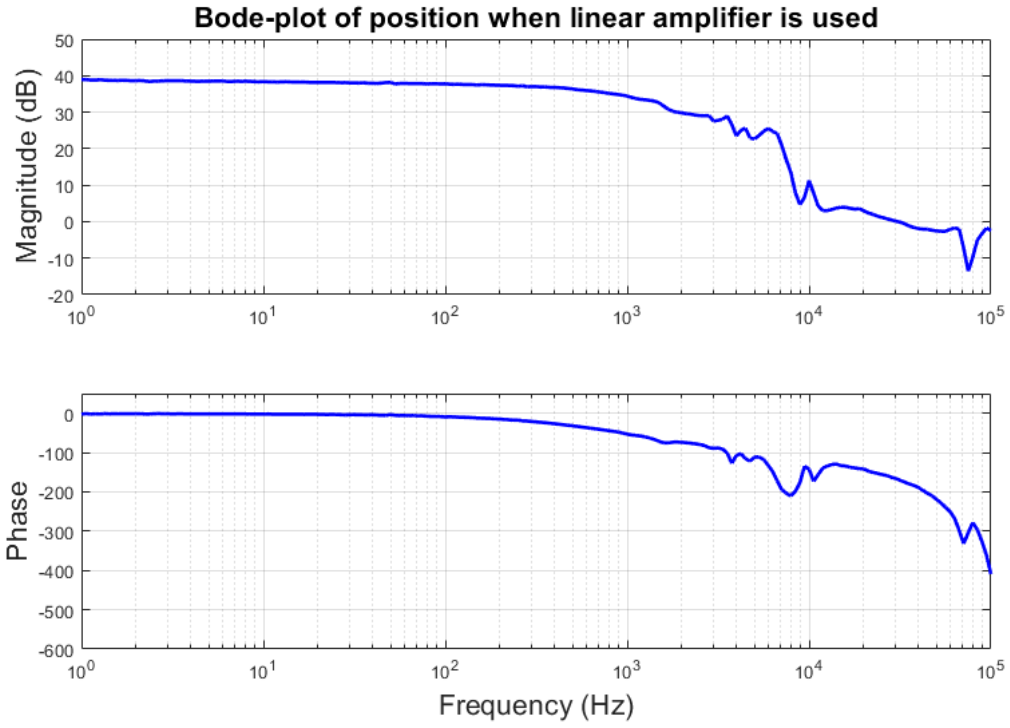

Figure 4.6: Bode-plot of position with the linear amplifier

4.2 Output Signal Distortion

As discussed in Chapter 1, a disadvantage of switching amplifiers in comparison with linear ones, is output current and voltage signal distortion. Main issues are current

and voltage ripples and nonlinearities caused by the dead-time. In this Section these concerns are investigated by increasing the switching frequency.

4.2.1 Voltage Ripple

In stationary case (input signal is constant DC voltage) and LC-filter is an output load of the half-bridge, mean values of current and voltage stay constant. Because of Equation (3.1), mean value of voltage on inductance has to be zero $\overline{u_L} = 0$. That also means that

$$\overline{v_{load}} = \overline{v_{out}} - \overline{u_L} = \overline{v_{out}} = D \cdot V_{bus}. \tag{4.1}$$

Current ripple of the load current is calculated from Equation (3.2) and then further used to calculate voltage ripple on the capacitor, because current ripple on the capacitor equals current ripple on the inductor. This is written as $\Delta i_C = \Delta i_L = \Delta i_{load}$. From equation

$$i_C = C\frac{du_C}{dt} \approx C\frac{\Delta u_C}{\Delta T}, \tag{4.2}$$

the voltage ripple is expressed as:

$$\Delta u_C = \frac{1}{8Cf_{sw}}\Delta i_{load}. \tag{4.3}$$

After substituting Δi_{load} with the values from Equation (3.2), voltage ripple is calculated as [17]:

$$\Delta u_C = \frac{DV_{bus}}{16LC} \cdot \frac{1}{f_{sw}^2}. \tag{4.4}$$

Figure 4.7 and 4.8 show output voltage v_{load} of piezoelectric actuator, when input reference voltage is a DC signal of 1 V. Figure 4.7 shows the voltage ripple for switching frequency of 225 kHz and Figure 4.8 voltage ripple for switching frequency of 1 MHz which is significantly reduced. In Figure 4.7 and 4.8 is also visible that shape of voltage signal is changed. When switching frequency is higher, the switching frequency harmonics are higher and hence filtering is higher. Voltage ripple due to the peak output voltage v_{out} on the bridge can be approximated by [3]:

$$\Delta u_C = V_{bus} \cdot \left(\frac{f_0}{f_{sw}}\right)^2 \tag{4.5}$$

where f_0 represents natural frequency of the output LC filter, $f_0 = 22\,\text{kHz}$. For $f_{sw} = 225kHz$ voltage ripple is

$$\Delta u_C = 20V \cdot \left(\frac{22kHz}{225kHz}\right)^2 = 191\,\text{mV}, \tag{4.6}$$

and for $f_{sw} = 1MHz$

$$\Delta u_C = 20V \cdot \left(\frac{22kHz}{1MHz}\right)^2 = 10\,\text{mV}. \tag{4.7}$$

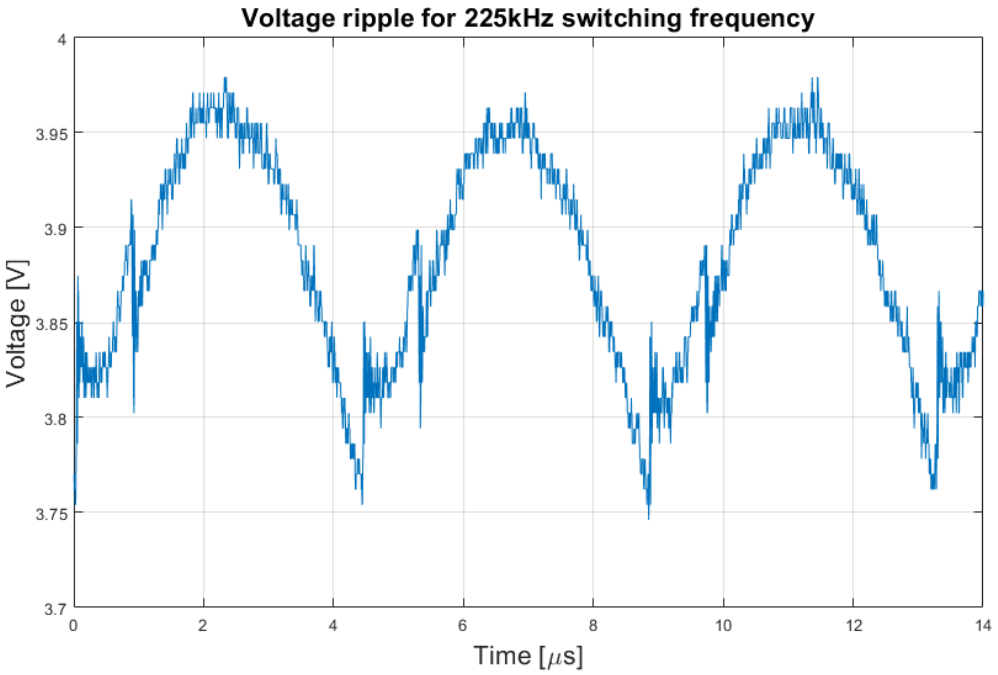

Figure 4.7: Voltage ripple when switching frequency is 225kHz

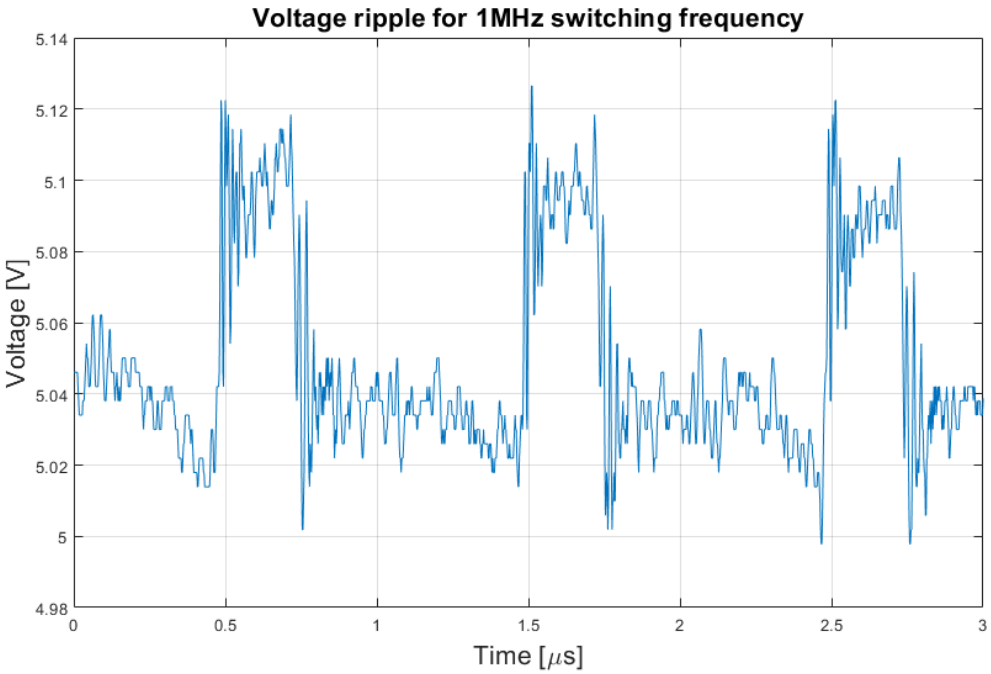

Figure 4.8: Voltage ripple when switching frequency is 1MHz

Calculated values correspond to values measured in Figure 4.7 and 4.8. It is noticeable that at higher switching frequencies, switching noise is more significant.

Switching noise at 1 MHz switching frequency is measured as more than 100 mV, which is around 10 times higher than voltage ripple. Switching noise is caused by parasites in the circuit and EMI.

For quantitative analysis, standard deviation (STD) of the voltage v_{load} is calculated. Figure 4.9 shows how standard deviation of output voltage v_{load} changes when switching frequency is increasing. The measurement corresponds to the Equation (4.4) up to the frequency of 450 kHz, where voltage is decreasing with increasing frequency. Afterwards, switching noise is increasing with switching frequency and standard deviation as well. It can be stated that switching frequency of 450 kHz reduces load voltage v_{load} STD the most, and has smallest switching noise influence, what is desirable in a nanopositioning system.

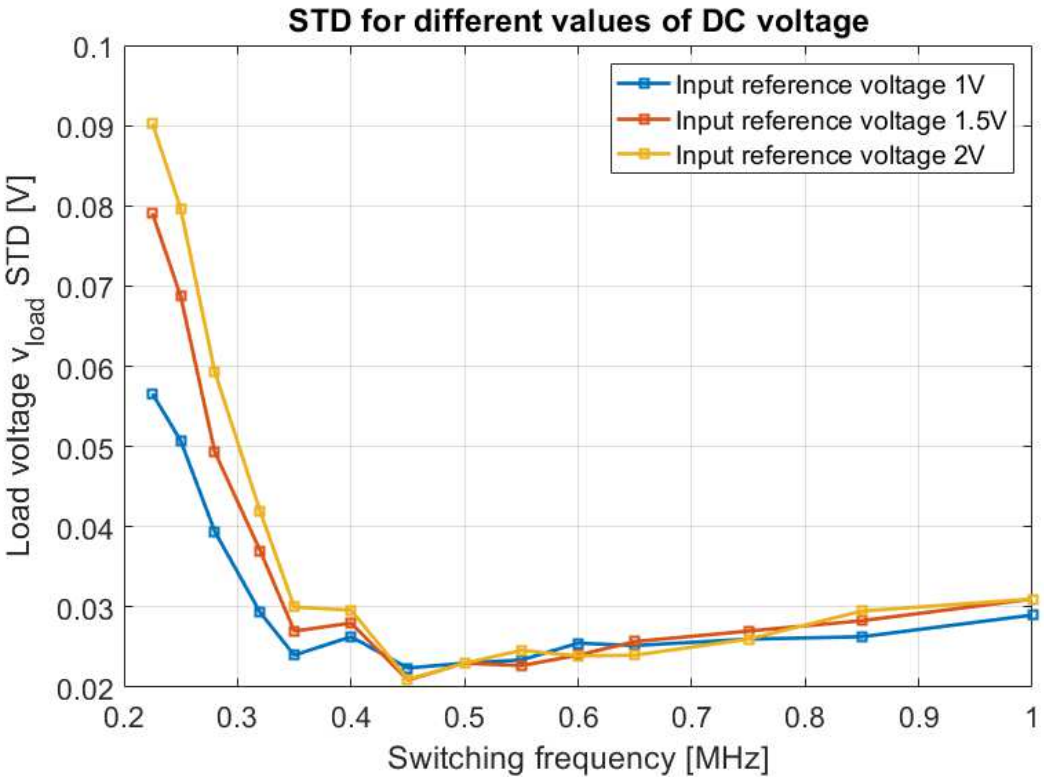

Figure 4.9: Change of standard deviation of output voltage v_{load} with increasing frequency

4.2.2 THD

The total harmonic distortion can be calculated by Equation (4.8). V_1 is RMS voltage value of the fundamental frequency and $V_2, V_3, \ldots$ are RMS voltage values of second, third,... signal harmonic.

$$THD = \frac{\sqrt{V_2^2 + V_3^2 + V_4^2 + \cdots}}{V_1} \tag{4.8}$$

Table 4.1: THD of the output voltage for different switching frequencies

Switching frequency	Input signal frequency	THD
250kHz	100Hz	1.26%
	1kHz	1.08%
	10kHz	1.51%
500kHz	100Hz	0.62%
	1kHz	1.27%
	10kHz	0.76%
750kHz	100Hz	1.67%
	1kHz	2.44%
	10kHz	2.68%

Linear or hybrid power amplifiers are often employed for high precision positioning applications, because nanoscale positioning applications require THD figures below $-90\,\mathrm{dB}$. In switching amplifiers THD is not significantly influenced by thermal dependency of $R_{DS(on)}$, but is sensitive to dead-time [18]. Odd-harmonics depend significantly on the dead-time, and THD which causes the output current distortion and is caused by odd-harmonics increases as the dead-time increases [18]. Dead-time introduced in the switching power amplifier is 7.5 ns and by measuring THD of the load voltage signal v_{load} its influence is investigated.

For calculation of THD first fifty harmonics ($V_2 - V_{50}$) are considered. To calculate THD values *Matlab* function *thd* is used. In Table 4.1 THD values for different switching frequencies are shown. It is visible that THD has lowest value in average at switching frequencies around $500kHz$, where standard deviation of the output voltage is also the lowest. Different THD values are consequence of different high frequency harmonic values for different switching frequencies, which excite resonances present in the system in different manner. THD of the output signal is additionally increased because of the hysteresis implemented in the PWM generator to remove chattering. Hysteresis introduces additional nonlinearities when the input signal is changing, hence calculated THD values are only approximate measure.

4.2.3 Noise Considerations

Requirements on an actuator current and voltage noise are high in precision positioning systems, because positioning stages have little damping and friction, so signal noise is easily transfered to position noise and creates undesired forces [18]. Therefore it is important to measure noise in the amplifier output voltage signal v_{load} and its influence to the positioning resolution.

Experiments are measured in a way that a reference DC signal is provided to the amplifier input, and this signal is amplified to generate the output signal to piezoelectric actuator v_{load}. This output signal voltage v_{load} is measured with the oscilloscope in 1 s time interval, and from measured value input position noise to the piezoelectric actuator is calculated. These values are given in Table 4.2, which shows

Table 4.2: Noise of the output voltage for different amplifiers

Output voltage v_{load}	Switching amplifier input positioning noise	Linear amplifier input positioning noise
0 V	18.5 nm_{pp}	11.1 nm_{pp}
10 V	19.7 nm_{pp}	20.9 nm_{pp}

noise comparison between linear power amplifier *Falco Systems WMA-300 High Voltage Amplifier DC-5MHz* (Falco Systems BV, Katwijk aan Zee, Netherlands) and developed switching power amplifier. When input reference signal is 0 V and output voltage on the load v_{load} is also 0 V, linear power amplifier has lower noise level, because switching power amplifier switching noise is already present. This noise level for the switching power amplifier does not change significantly even when input reference signal is increased, so that the $v_{load} = 10$ V. Compared to that, noise of the linear power amplifier is doubled when it generates output voltage $v_{load} = 10$ V. Noise in linear power amplifiers arises from stochastic signals that are generated in resistances and all other amplifier components [3]. Linear power amplifier noise is influenced by voltage and current values, since higher temperature drift appears at higher voltage and current values. High-frequency switching power amplifier for higher input voltages generates noise similar to the one generated by linear power amplifier.

4.3 Power Dissipation

Similar to the analysis in Section 3.2, power dissipation of the FETs is considered with the piezoelectric actuator attached to the output of the switching power amplifier. For the measurement infrared camera as in Section 3.2 is used, and the same procedure is repeated. Temperature is measured to determine influence of switching frequency. For the measurement, half-bridge voltage is $V_{bus} = 20$ V and load current is shown in Figure 4.12. Load current is switching and changing direction from positive to negative as the energy is transferred from inductance to capacitor and opposite. Absolute value of current at its peak in the switching moment reaches more than 200 mA, and RMS current value is comparable to the measurements conducted with inductive load.

Figures 4.10 and 4.11 show measured temperatures when the switching frequency is 225 kHz and 500 kHz respectively. It is noticeable that increasing the frequency by 275 kHz resultes in a increase in temperature for more than 40 °C. Equation (3.4) is used to calculate power dissipation of the FET, when piezoelectric load is attached to the output. For switching frequency of 225 kHz and temperature 53.1 °C power dissipation is $P_{loss1} = 0.35$ W and for switching frequency of 500 kHz and temperature 95.2 °C power dissipation is $P_{loss2} = 0.85$ W. Meaning that increase in power dissipation for 0.5 W caused temperature increase of 40 °C. Figure 4.13 shows linear temperature increase for linearly increasing switching frequency. Blue line shows experimentally measured values when piezoelectric actuator is attached to

the output stage of the amplifier, and red dashed line shows the linear trend line.

Although the FET temperature has significantly increased in comparison to measured temperatures in Section 3.2, power dissipation of the GaN-based switching power amplifier did not yet reach the power dissipation of linear and standard switching power amplifier mentioned in Table 3.1. Slope of the linear trend line in Figure 4.13 has significantly increased in comparison to the one measured in Figure 3.11 which clearly shows that energy losses due to switching have increased. To evaluate the measurement results, hard switching is considered.

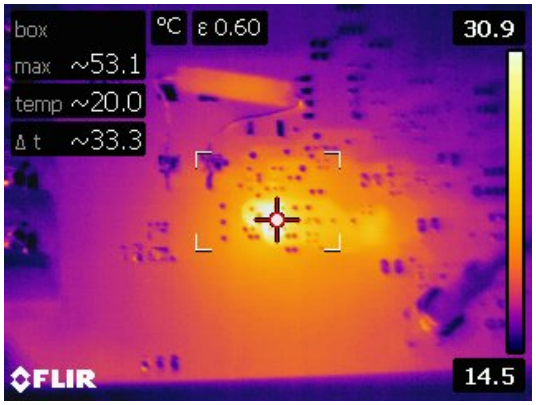

Figure 4.10: Temperatures at 225kHz switching frequency

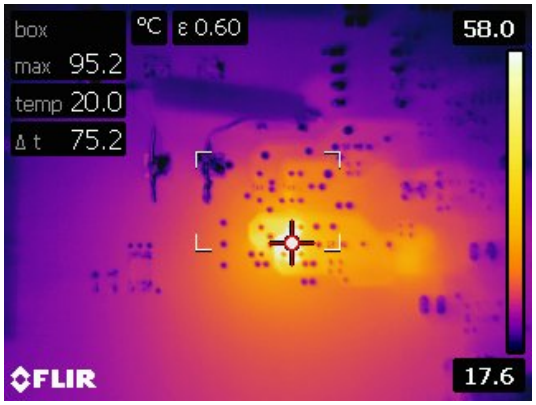

Figure 4.11: Temperatures at 500kHz switching frequency

4.4 Hard Switching for Piezoelectric Load

Equation (3.8) is defined for inductive load attached to the output of the switching power amplifier, thus it cannot be used to determine switching condition for piezoelectric actuator attached to the power amplifier output. Energy loss model is derived under assumption that current is constant during the PWM cycle [18]. Figure 4.12 shows load current going through the LC low pass filter when switching frequency is 225 kHz and bus voltage applied is $V_{bus} = 20\,\text{V}$. It is visible that current is significantly changing during one switching cycle.

To determine the system behavior at switching transition, Q factor of the LC_{oss} resonant circuit is calculated, since it determines how high is the resonance of that circuit during the dead-time:

$$Q = R_{DS(on)}\sqrt{\frac{C_{oss}}{L}} \tag{4.9}$$

$$Q = 70m\Omega\sqrt{\frac{150pF}{47\mu\text{H}}} \tag{4.10}$$

$$Q = 0.125 \cdot 10^{-3} \tag{4.11}$$

From calculated Q factor value can be stated that resonance of the LC_{oss} circuit is highly damped, so no high current peaks are occurring during the dead-time. During

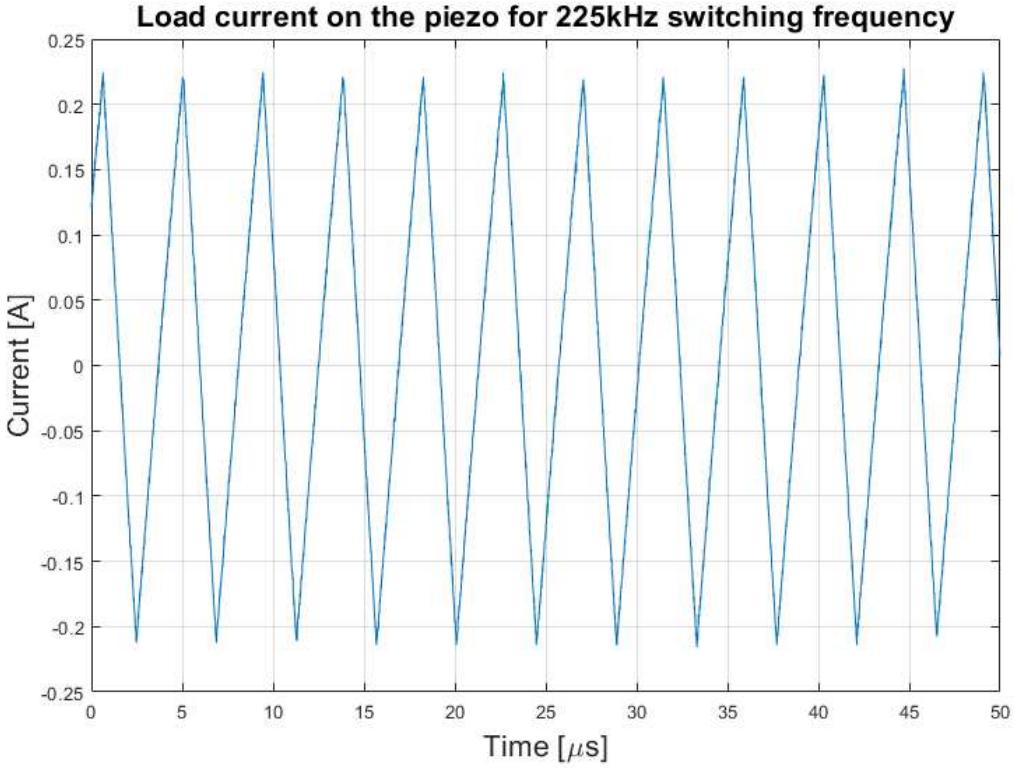

Figure 4.12: Load current when switching frequency is 225 kHz

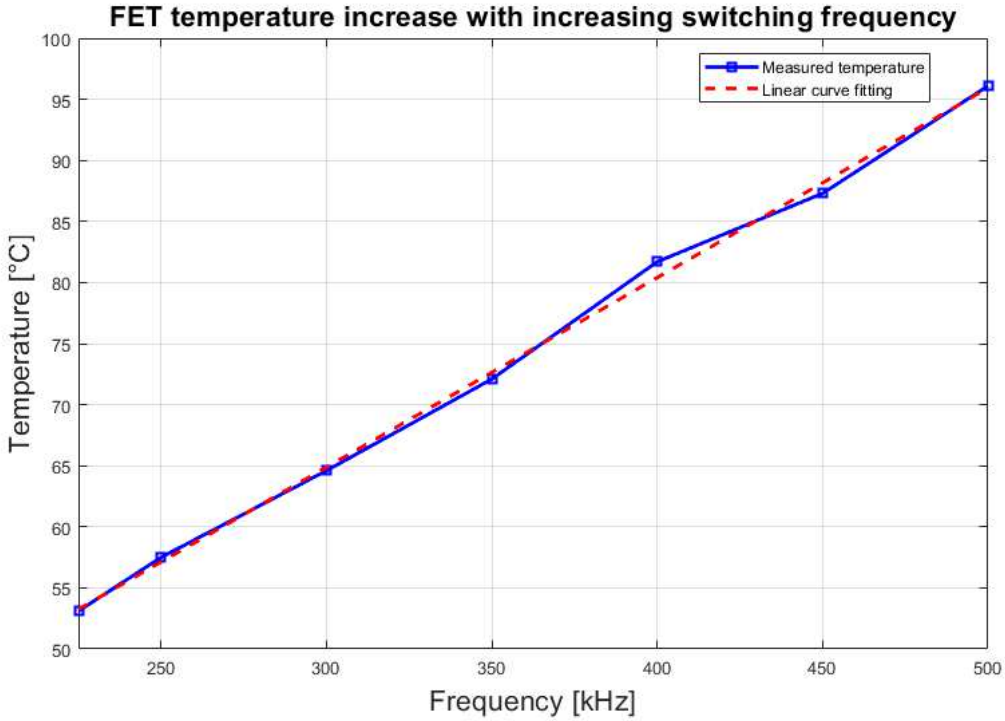

Figure 4.13: Increase of FET temperature with increasing switching frequency

the dead-time, transistor voltage slope V_{DS} is determined by the current level and the parasitic capacitor value [3]. Piezoelectric capacitor of the output filter can be observed as a voltage source, as the voltage over the piezoelectric capacitor will change only very little within one switching cycle of the high-frequency current [3]. While voltage is changing, the energy in the inductor flows partly into the parasitic capacitor and dynamic behaviour is determined by the parasitic capacitor and the inductor and their natural resonating mode [3]. Resonance of the parasitic capacitance and inductor is

$$\omega = \frac{1}{\sqrt{LC_{oss}}} = 11.9 \cdot 10^6 \frac{rad}{s} \tag{4.12}$$

$$T = \frac{2\pi}{\omega} = 528ns \tag{4.13}$$

From the measured dead-time $T_d = 7.5\,\text{ns}$ it is visible that $T/2 \gg T_d$. Therefore, parasitic capacitance is only partially discharged during the dead-time and current spike due to hard switching is appearing. As a consequence parasitic capacitor discharges internally in the FET, and hard switching causes that channel temperature is increased significantly by self-heating [41]. Energy losses per switching event increase significantly when GaN FET is hard switching [40]. This is noticed in measurement results in Section 4.3, as increased slope of the linear trend line in Figure 4.13, and relatively high measured temperatures, even at lower switching frequencies.

4.5 Evaluation of Piezoelectric Actuator Motions

Piezoelectric actuators are used in precision positioning stages and they have nanometer resolution in a small motion range. Piezoelectric actuator used in scanning unit is often driven in a triangular scanning motion, so for experimental evaluation, triangular wave is used as an input signal. Figure 4.14 shows measured position of piezoelectric actuator when it is driven by switching power amplifier with switching frequency of 750 kHz. To calculate position from output voltage v_{load} on piezoelectric actuator in μm, maximum range 19.8 µm of the actuator is divided by maximum voltage 150 V which can be applied to piezoelectric actuator and multiplied by currently measured voltage v_{load}. Calculated position is shown by red line in Figure 4.14. To measure actual position of the piezoelectric actuator, shown by blue line in Figure 4.14, interferometer $IDS3010$ is used, as described in Chapter 2. Output voltage of interferometer is decoded by FPGA and decoded signal forwarded to the output of the DAC of FPGA, where it is measured as a voltage signal. To retrieve actual position of piezoelectric actuator, measured voltage is multiplied by factor 200 pm/1 mV.

Figure 4.15 shows position signals of piezoelectric actuator when it is driven by linear power amplifier *Falco Systems WMA-300 High Voltage Amplifier DC-5MHz*. Difference can be noticed when comparing red lines in Figure 4.14 and 4.15. Bandwidth of the linear power amplifier is 1 kHz, hence the higher harmonics of input

triangular signal, starting from the second one which has frequency $3 \cdot f_0 = 1.5\,\text{kHz}$, are damped. This results in damped amplitude of position signal calculated from output voltage v_{load}, and eventually in the amplitude of moving actuator. It is also noticeable that measured position signal in Figure 4.15 is more noisy than signal in Figure 4.14. This can be related with the LC low pass filter attached to the output stage of the switching power amplifier, which filters high frequency harmonics in current and voltage signal.

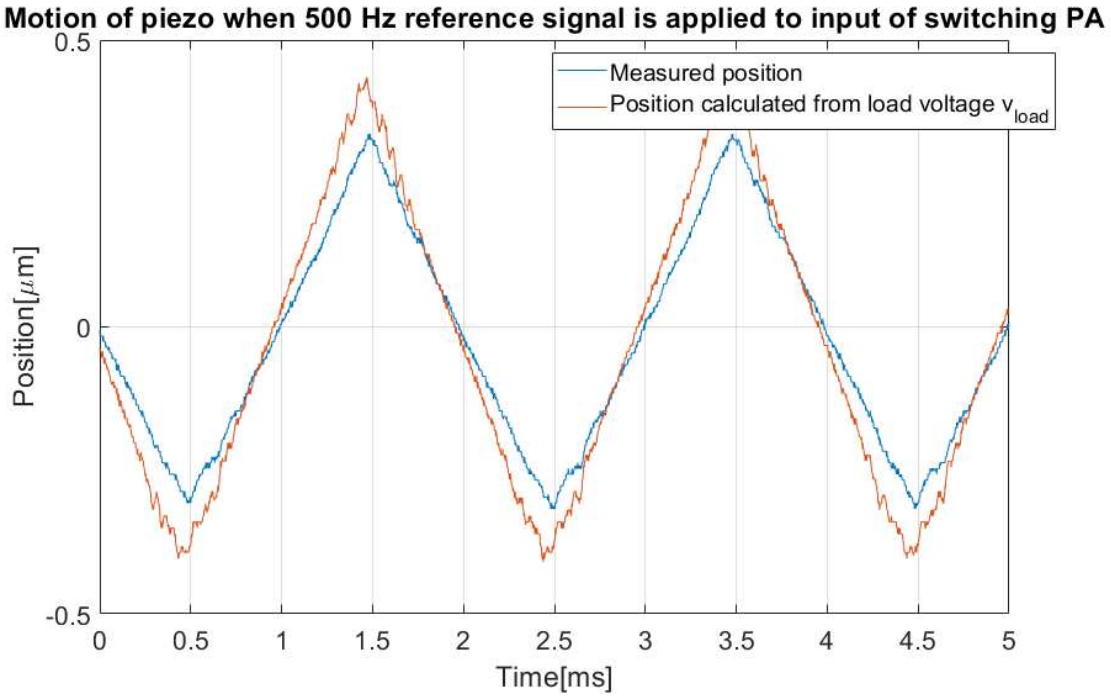

Figure 4.14: Motion of piezoelectric actuator when driven by switching power amplifier

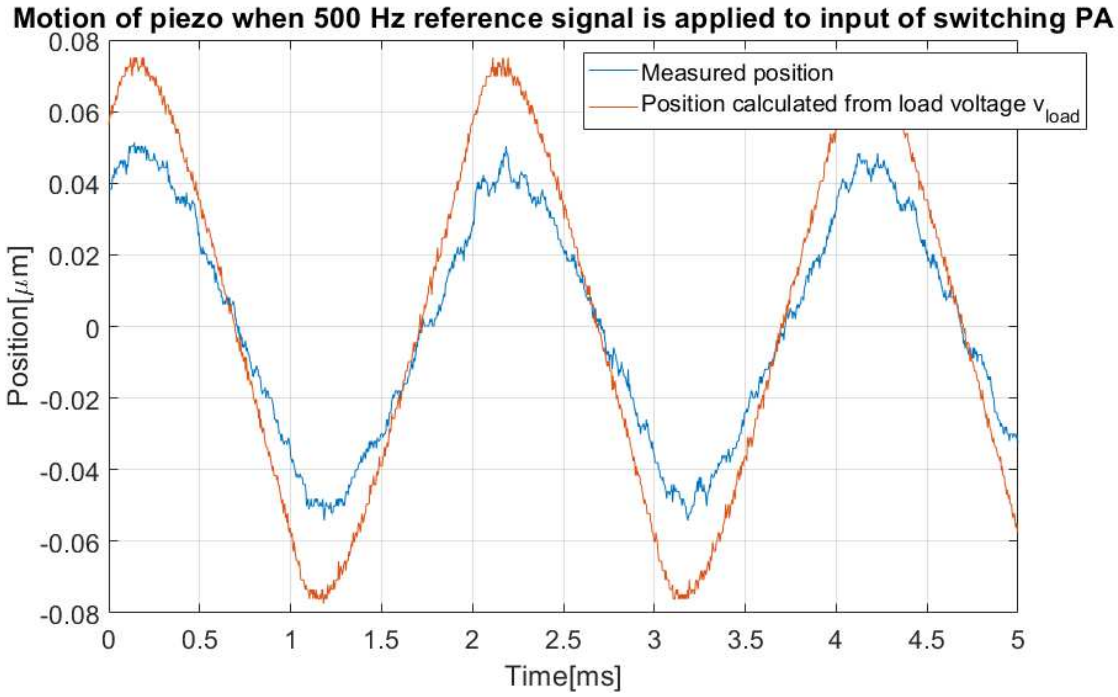

Figure 4.15: Motion of piezoelectric actuator when driven by linear power amplifier

CHAPTER 5

Conclusion

5.1 Summary

For energy efficient, high resolution positioning of a piezoelectric actuator, GaN-based power amplifier is designed and developed, which is described in Chapter 2. The switching power amplifier consists of four parts. For output stage transistors GaN FETs are selected because they enable high switching frequency, and a PCB is designed for the required high voltage and current of piezoelectric actuator. Newly developed GaN FETs have much better figure of merit than typical MOSFETs. GaN FET low value of parasitic capacitance $C_{oss} = 64\,\text{pF}$, gate charge $Q_G = 1\,\text{nC}$ and zero reverse recovery charge Q_{RR}, have allowed driving the transistors with shorter dead-time at higher switching frequencies. Transistors with better switching performance are used to reduce influence of noise and distortion on positioning resolution. The other three amplifier parts, the PWM generator, the gate driving circuit and LC filter, are designed and developed to provide switching frequencies up to 1 MHz and to reduce output signal distortion.

To evaluate performance of the high-frequency switching power amplifier experiments with the gate driving circuit and output stage with inductive load $L = 24.76\,\text{mH}$ and $R = 24\,\Omega$ are conducted and results are discussed in Chapter 3. Output stage voltage signals V_{GS} and V_{DS} are first measured in order to examine the gate driving circuit working conditions and afterwards, change of current ripple and temperature with increasing switching frequency is measured.

For evaluation of the amplifier with piezoelectric actuator in Chapter 4, different input signal waveforms are generated. For that reason PWM generator is implemented and its output is used as input signal to gate driving circuit. LC-filter, with $L = 47\,\mu\text{H}$ and $C = 1.1\,\mu\text{F}$ given as capacitiance of piezoelectric actuator, is attached to the output of the amplifier for the high frequency harmonics damping and interferometer is used to provide motion information. To determine system dynamic properties Bode-plots from input voltage to output voltage and position

are measured. Voltage ripple and temperature change with increasing switching frequency is measured and measurements are used to evaluate system performance.

5.2 Conclusion

The experiments using the inductive load clearly demonstrates the advantages of the fast switching. Particularly, the increase of the switching frequency from 20 kHz to 1 MHz significantly decreases the current ripple of the coil current by a factor of 13. Furthermore, the measured temperature reveals that the developed GaN-based switching amplifier realizes a significantly smaller energy dissipation, which is approximately 10 times and 60 times lower than a conventional switching amplifier and a typical linear amplifier, respectively. Consequently, a high-frequency switching amplifier is beneficial to simultaneously improve the positioning resolution and the energy efficiency of a motion system with electromagnetic actuators (e.g. Lorentz actuators).

In the case of the piezoelectric actuator, the high-frequency switching is beneficial for a high positioning bandwidth. Due to the fast switching frequency of more than 225 kHz, the bandwidth of the switching amplifier that is determined by the LC filtering can be more than 22 kHz, which is sufficiently higher than the first mechanical resonance of the piezoelectric actuator (6 kHz). Thus, the GaN-based switching amplifier does not restrict the positioning bandwidth of the piezoelectric actuator. The experiments also reveal that the voltage ripple of the piezoelectric actuator can be decreased by the switching frequency up to 450 kHz. This demonstrates another advantage of the high-frequency switching. However, the energy dissipation is relatively high when the piezoelectric actuator is used. The measured temperature of the transistor increases from 53.1 $^{\circ}C$ to 95.2 $^{\circ}C$ when the switching frequency changes from 225 kHz to 500 kHz. The analysis has revealed that the high energy losses when driving the piezoelectric actuator occur due to hard switching of the transistors.

Overall, the high-frequency switching amplifiers are beneficial for electromagnetic actuators by realizing low current ripple, high energy efficiency, and high bandwidth. For piezoelectric actuators, hard switching is the major problem for energy efficiency while increasing switching frequency to effectively improve the bandwidth and decrease the voltage ripple.

5.3 Future Work

To simultaneously realize the high energy efficiency, the low voltage ripple, and the high bandwidth of a switching amplifier, remedies against the hard switching of the transistors will be indispensable in future work. For example, dead-time could be increased or control of the resonant-mode output stage [3] could be implemented.

Bibliography

[1] S. Pirker, *Improving Positioning Performance of a PWM-Driven System by Applying a Mechatronic Solution.* pp.57-60: Automation and Control Institute, Master's thesis, 2015.

[2] G. Schitter, P. Thurner, and P. Hansma, *Design and input-shaping control of a novel scanner for high-speed atomic force microscopy*. pp. 282–288: Mechatronics, 18(5-6), 2008.

[3] R. M. Schmidt, G. Schitter, and J. van Eijk, *High Performance Mechatronics*. Delft University Press, 2011.

[4] B. Whatley, J. Kuo, C. Shuai, B. Damon, and X. Wen, *Fabrication of a biomimetic elastic intervertebral disk scaffold using additive manufacturing.* pp. 015004: Biofabrication, 3(1), 2011.

[5] G. Schitter and N. Phan, *Field programmable analog array (FPAA) based control of an atomic force microscope.* pp. 2690-2695: American Control Conference. IEEE., 2008.

[6] S. Salapaka, A. Sebastian, J. Cleveland, and M. Salapaka, *High bandwidth nano-positioner: A robust control approach*. pp. 3232–3241: Review of scientific instruments, 73(9), 2002.

[7] A. Fleming, *A megahertz bandwidth dual amplifier for driving piezoelectric actuators and other highly capacitive loads.* pp.104701: Review of Scientific Instruments, 80(10), 2009.

[8] G. Schitter and M. Rost, *Scanning probe microscopy at video-rate*. pp.40–48: Materials Today, 11, 2008.

[9] E. Csencsics, J. Schlarp, and G. Schitter, *High-Performance Hybrid-Reluctance-Force-Based Tip/Tilt System: Design, Control, and Evaluation.* pp.2494-2502: IEEE/ASME Transactions on Mechatronics, 23(5), 2018.

[10] H. Yoo, S. Ito, and G. Schitter, *High speed laser scanning microscopy by iterative learning control of a galvanometer scanner.* pp.12-21: Control Engineering Practice, 50, 2016.

[11] S. Maniktala, *Switching Power Supplies A-Z.* Elsevier, 2012.

[12] P. Gupta, N. Pradhan, and S. Jana, *Design of CMOS based Class-A Power Amplifier for C-Band applications*. pp. 1–4: International Symposium on Devices, Circuits and Systems. IEEE., 2018.

[13] H. Choi, *Prelinearized Class-B Power Amplifier for Piezoelectric Transducers and Portable Ultrasound Systems. Sensors*. pp. 287: Sensors, 19(2), 2019.

[14] C. Stiebel and H. Janocha, *New concept of a hybrid amplifier for driving piezoelectric actuators*. pp. 365–370: IFAC Proceedings Volumes, 33(26), 2000.

[15] K. Wiedmann, F. Wallrapp, and A. Mertens, *Analysis of inverter nonlinearity effects on sensorless control for permanent magnet machine drives based on high-frequency signal injection.* pp. 1–10: Power Electronics and Applications, European Conference on, 2009.

[16] A. D. Saha and V. John, *Analysis and Modelling of Non-idealities in High Frequency Class D Amplifier.* pp. 44–49: Electrical Energy Systems, International Conference on, 2016.

[17] F. Zach, *Leistungselektronik: Ein Handbuch, Bande 1 und Band 2.* Springer-Verlag (Vol. 2), 2015.

[18] M. Mauerer and J. Kolar, *Distortion minimization for ultra-low THD class-D power amplifiers*. pp.324–338: CPSS Transactions on Power Electronics and Applications, 3(4), 2018.

[19] Datasheet, "EPC2012C, Enhancement Mode Power Transistor." [Online]. Available: https://www.irf.com/product-info/audio/classdtutorial606.pdf

[20] R. Bakker and M. Duffy, *Maximising the efficiency of a Class-D audio amplifier output stage*. pp.1–5: Irish Signals and Systems Conference. IEEE, 2017.

[21] I. Rossetto, M. Meneghini, A. Tajalli, S. Dalcanale, C. D. Santi, P. Moens, A. Banerjee, E. Zanoni, and G. Meneghesso, *Evidence of hot-electron effects during hard switching of AlGaN/GaN HEMTs.* pp.3734-3739: IEEE transactions on electron devices, 64(9), 2017.

[22] E. Jones and A. Pozo, *Hard-Switching Dynamic R ds, on Characterization of a GaN FET with an Active GaN-Based Clamping Circuit.* pp. 2757-2763: Applied Power Electronics Conference and Exposition. IEEE., 2019.

[23] J. Roig and F. Bauwens, *Origin of Anomalous C_{OSS} Hysteresis in Resonant Converters With Superjunction FETs.* pp.3092-3094: IEEE Transactions on Electron Devices, 62(9), 2015.

[24] Z. Lin, *Study on the Intrinsic Origin of Output Capacitor Hysteresis in Advanced Superjunction MOSFETs.* pp.1297-1300: IEEE Electron Device Letters, 40(8), 2019.

[25] M. Shen and S. Krishnamurthy, *Simplified loss analysis for high speed SiC MOSFET inverter.* pp. 1682-1687: Twenty-Seventh Annual IEEE Applied Power Electronics Conference and Exposition, 2012.

[26] Datasheet, "NAC2013-HXX." [Online]. Available: http://www.noliac.com/products/actuators/plate-stacks/show/nac2013-hxx

[27] U. manual, *attoSENSORICS, User Manual IDS3010.* Firmware version: 1.4.0: Manual version: 1.4.0, 2017.

[28] M. Kasper, R. Burkart, G. Deboy, and J. Kolar, *ZVS of power MOSFETs revisited.* pp.8063-8067: IEEE Transactions on Power Electronics, 31(12), 2016.

[29] R. Miftakhutdinov, *Analysis and practical method of determining WBG FET switching losses associated with nonlinear coss.* pp. 974-978: IEEE Applied Power Electronics Conference and Exposition, 2017.

[30] P. S. Paper, "The GaN Opportunity - Higher Performances and New Challenges." [Online]. Available: https://www.power-mag.com/pdf/feature_pdf/1319704820_National0611_Layout_1.pdf

[31] M. Berkhout, *An Integrated 200-W Class-D Audio Amplifier.* pp. 1198–1206: IEEE Journal of Solid-State Circuits, 38(7), 2003.

[32] C. Ku, C. Chen, Y. Hsu, and M. Sun, *Experience in simulation and measurement of GaN FET switching behavior.* pp. 400-405: International Future Energy Electronics Conference and ECCE Asia. IEEE., 2017.

[33] A. Report, "PCB Design Guidelines for 0.5mm Package-on-Package Applications Processor, Part I." [Online]. Available: http://www.ti.com/lit/an/sprabb3/sprabb3.pdf

[34] A. note, "Assembling eGaN FETs." [Online]. Available: https://www.digikey.com/en/pdf/e/epc/epc-appnote-gan-assembly

[35] J. Caldwell, "Analog Pulse Width Modulation." [Online]. Available: http://www.ti.com/lit/ug/slau508/slau508.pdf

[36] Datasheet, "200MHz, CMOS operational amplifier." [Online]. Available: https://www.ti.com/lit/ds/symlink/opa356.pdf

[37] C. Datasheet, "TLV350x, 4.5ns Rail to Rail High Speed Comparator." [Online]. Available: https://www.ti.com/lit/ds/symlink/tlv3501.pdf

[38] L. Yang, L. Xu, T. Yang, and B. Zhang, *Class D power amplifier for audio beam system.* pp. 3469-3474: International Conference on Mechatronics and Automation. IEEE., 2007.

[39] A. Note, "Accurately Measuring High Speed GaN Transistors." [Online]. Available: https://epc-co.com/epc/Portals/0/epc/documents/application-notes/AN023%20Accurately%20Measuring%20High%20Speed%20GaN%20Transistors.pdf

[40] W. paper WP012, "Dead-Time Optimization for Maximum Efficiency." [Online]. Available: https://epc-co.com/epc/Portals/0/epc/documents/papers/Dead-Time%20Optimization%20for%20Maximum%20Efficiency.pdf

[41] J. Joh, N. Tipirneni, S. Pendharkar, and S. Krishnan, *Current collapse in GaN heterojunction field effect transistors for high-voltage switching applications.* pp. 6C-5: IEEE International Reliability Physics Symposium, 2014.

[42] S. Bahl, D. Ruiz, and D. Lee, *Product-level reliability of GaN devices.* pp. 4A-3: IEEE International Reliability Physics Symposium, 2016.

Appendix A

1 PCB Layout

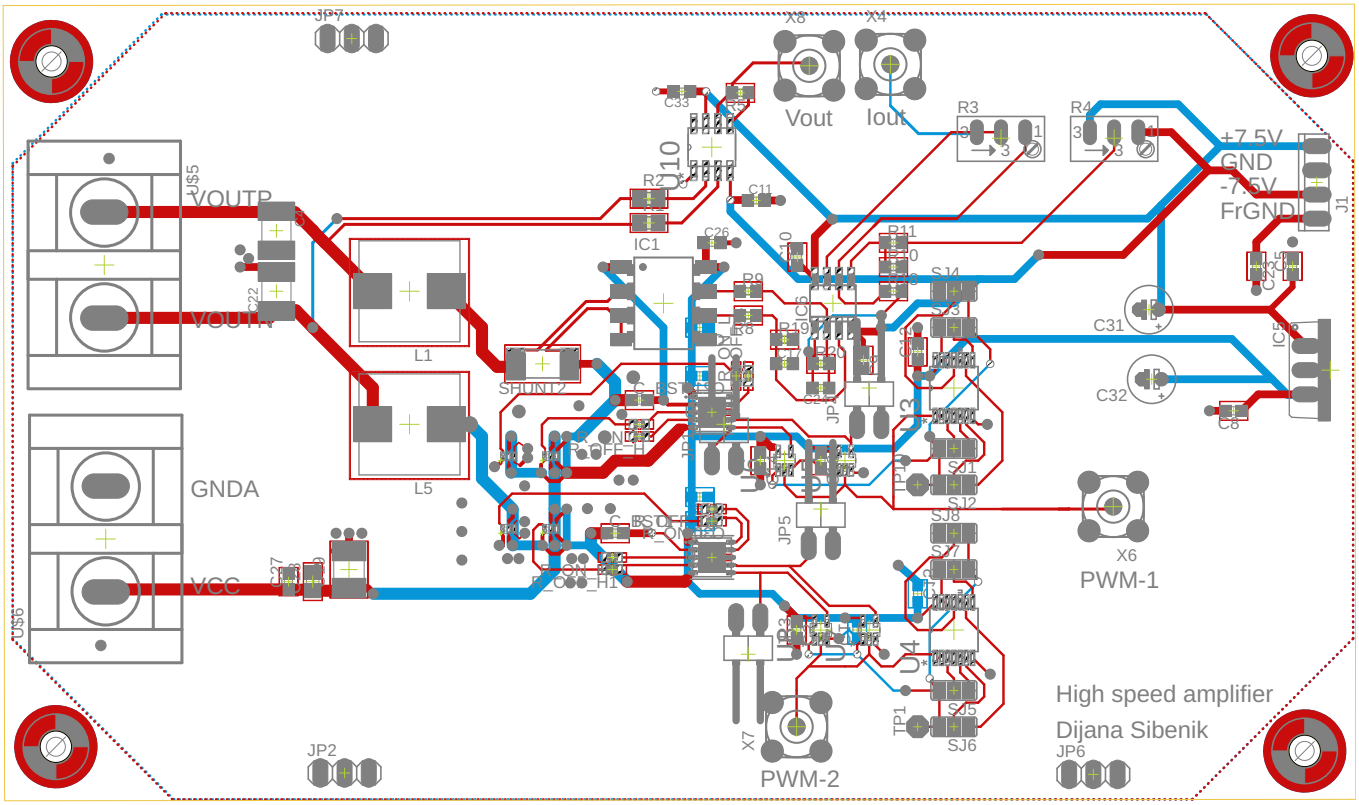

Erklärung

Hiermit erkläre ich, dass die vorliegende Arbeit gemäß dem Code of Conduct, insbesondere ohne unzulässige Hilfe Dritter und ohne Benutzung anderer als der angegebenen Hilfsmittel, angefertigt wurde. Die aus anderen Quellen direkt oder indirektübernommenen Daten und Konzepte sind unter Angabe der Quelle gekennzeichnet.
Die Arbeit wurde bisher weder im In- noch im Ausland in gleicher oder in änilcher Form in anderen Prüfungsverfahren vorgelegt.

Datum: 15.12.2019.

Unterschrift